Supporting Information

Tetraphenylbutadiene-Based Symmetric 3D Hole-Transporting Materials for Perovskite Solar Cells: A Trial Trade-off between Charge Mobility and Film Morphology

Jian Chen,[†,§,#] Jianxing Xia,[‡,#] Wei-Jie Gao,[†] Hui-Juan Yu,[†,§,∥] Jun-Xing Zhong,[†] Chunyang Jia,[‡] Yuan-Shou Qin,[⊥] Zhigang She,[†] Dai-Bin Kuang,[†] and Guang Shao*[,†,§,∥]

[†]School of Chemistry, Sun Yat-sen University, Guangzhou, 510275, China. E-mail: shaog@mail.sysu.edu.cn

[‡]State Key Laboratory of Electronic Thin Films and Integrated Devices, School of Electronic Science and Engineering, University of Electronic Science and Technology of China, Chengdu, 610054, China

[§]Shenzhen Research Institute, Sun Yat-sen University, Shenzhen, 518057, China

[∥]South China Advanced Materials Science & Technology (Guangzhou) Company Limited, Guangzhou, 511400, China

[⊥]Zeloq (Hunan) Technology Company Limited, Yiyang, 413200, China

[#]These authors contributed equally to this work.

Table of Contents

1. Materials, instruments, and methods

All chemicals were obtained from commercial suppliers and used as received without further processing, unless specially stated. All reactions were carried out in Ar atmosphere, unless otherwise pointed out. All dry reactions were carried out with glassware flamed under vacuum and backfilled with Ar. Solvents were dried based on the standard procedures. Column chromatography was conducted with silica gel (300–400 mesh). Thin-layer chromatography was performed with silica gel GF254 pre-coated on glass and visualized under UV light (254 or 365 nm). ^{1}H and ^{13}C NMR spectra were recorded at 25 ℃ on a Bruker AVANCE III 300, 400, or 500 MHz nuclear magnetic resonance (NMR) spectrometer. Chemical shifts are reported in parts per million (ppm) relative to internal standards (TMS, 0 ppm for ^{1}H NMR; $CDCl_3$, 77.00 ppm for ^{13}C NMR; and 85% phosphoric acid, 0 ppm for ^{31}P NMR). Coupling constants (*J*) are given in Hz. Multiplicities are denoted as below: s = singlet, d = doublet, t = triplet, q = quartet, m = multiplet, br = broad. The peak at ~1.57 ppm is the signal of protons from H_2O, which is the common residue in $CDCl_3$.[1] HRMS spectra were recorded on a Bruker ESI-Q-TOF maXis 4G mass spectrometer using electrospray ionization (ESI) technique. X-ray diffraction data were gleaned on an Agilent SuperNova diffractometer with Cu K_α radiation (λ = 1.54184 Å) or Mo K_α radiation (λ = 0.71073 Å) at 150 K using ω scans method. Computations were implemented by the Gaussian 09W software within the framework of Density Functional Theory (DFT) adopting the B3LYP exchange correlation functional and 6-31G basis set.[2] The calculated results were visualized by the GaussView software.[3] UV–vis absorption spectra were measured with a SHIMADZU UV-3600 UV–VIS–NIR spectrometer.

Steady-state photoluminescence (PL) spectra and time-resolved PL spectra were recorded on a SHIMADZU RF-5301PC or Edinburgh Instruments FLS980 spectrometer. In time-resolved PL measurements, a pulsed laser with wavelength of 406.2 nm and pulse width of 58.8 ps was used as an excitation source. Cyclic voltammetry (CV) were conducted with a Zahner Zennium electrochemical workstation using a three-electrode electrochemical cell. Tetrabutylammonium hexafluorophosphate (0.1 M) was used as electrolyte, a $Ag/AgNO_3$ (0.01 M in acetonitrile) electrode was used as reference, a platinum wire was used as working electrode, and a platinum sheet was used as counter electrode. Prior to the tests, the sample solutions were deoxygenated by Ar for 10 min each. The sweep rate was 50 mV/s. Thermogravimetric analysis (TGA) was explored with a NETZSCH STA 449 F3 Jupiter thermogravimetric analyzer in the range of 35–900 ℃ (10 K/min, N_2 atmosphere). Differential scanning calorimetry (DSC) was scrutinized by a NETZSCH 204 F1 Phoenix differential scanning calorimeter (10 K/min, N_2 atmosphere). Water contact angles were measured on a Krüss DSA 100 drop shape analyzer. The cross-sectional picture of cell and top-view pictures of doped HTM films spin-coated on $MAPbI_3$ were taken by a Hitachi SU8010 field-emission scanning electron microscope (SEM). Topography of doped HTM films spin-coated on $MAPbI_3$ was acquired with a Bruker MultiMode 8 atomic force microscope (AFM) in ScanAsyst mode.

2. Synthesis of intermediates

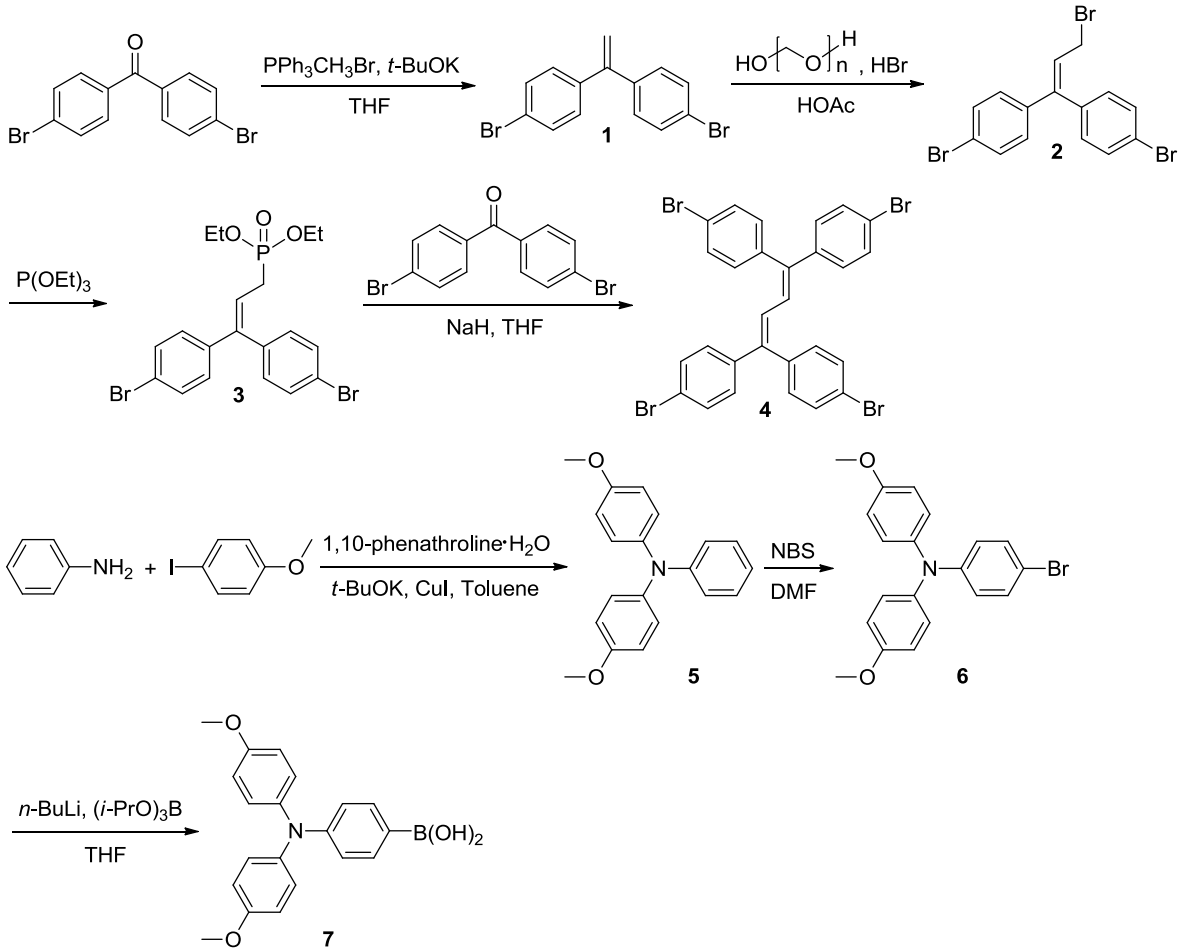

Scheme S1. Synthetic route to intermediates **1**–**7**.

(1) Synthesis of **1**

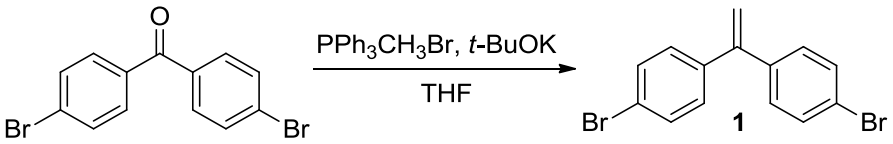

4,4′-dibromobenzophenone (1700.1 mg, 5.000 mmol, 1.00 equiv.), methyltriphenylphosphonium bromide (3574.7 mg, 10.007 mmol, 2.00 equiv.), potassium *tert*-butoxide (1129.1 mg, 10.062 mmol, 2.01 equiv.), and THF (20 mL) were placed in a two-necked round flask and stirred at room temperature for 39.5 h in an Ar atmosphere. After that, the solvent was evaporated under a reduced pressure. The crude product was purified by column chromatography with petroleum ether/ethyl acetate (50/1, v/v) as eluent

to obtain product as a white solid (1257.0 mg, 74.37%). ^{1}H NMR (300 MHz, $CDCl_3$): δ (TMS, ppm) = 7.47 (d, J = 9.0 Hz, 4H), 7.18 (d, J = 9.0 Hz, 4H), 5.46 (s, 2H), coinciding with the reported data.[4]

(2) Synthesis of **2**

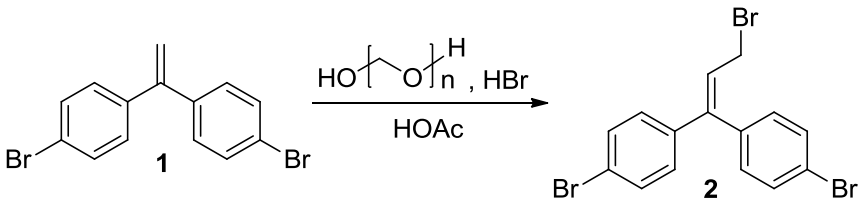

1 (343.5 mg, 1.016 mmol, 1.00 equiv.), paraformaldehyde (46.0 mg), hydrogen bromide solution (33 wt. % in acetic acid, 0.3 mL, 1.657 mmol, 1.63 equiv.), and acetic acid (4 mL) were placed in a two-necked round flask and stirred at 50 ℃ for 27.5 h in an Ar atmosphere. After that, water was added to the mixture. Then the mixture was extracted with CH_2Cl_2 (DCM). The extracts were dried by anhydrous magnesium sulfate, filtered, and evaporated under a reduced pressure. The crude product was purified by column chromatography with petroleum ether/ethyl acetate (50/1, v/v) as eluent to obtain product as a white oil (404.2 mg, 92.31%).^{1}H NMR (400 MHz, $CDCl_3$): δ (TMS, ppm) = 7.56 (d, J = 8.0 Hz, 2H), 7.42 (d, J = 8.0 Hz, 2H), 7.13 (d, J = 8.0 Hz, 2H), 7.08 (d, J = 8.0 Hz, 2H), 6.33 (t, J = 8.0 Hz, 1H), 3.99 (d, J = 8.0 Hz, 2H). ^{13}C NMR (100 MHz, $CDCl_3$): δ (ppm) = 143.88, 139.52, 136.40, 131.82, 131.47, 131.06, 129.16, 124.65, 122.55, 122.39, 30.12.

(3) Synthesis of **3**

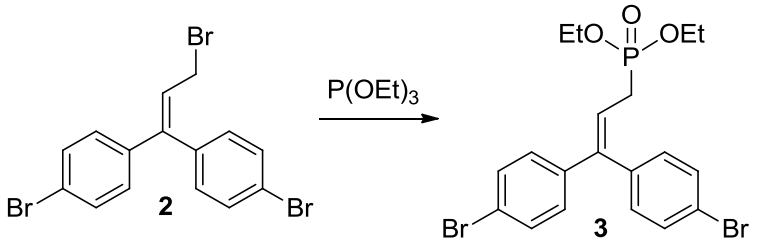

2 (448.0 mg, 1.040 mmol, 1.00 equiv.) and triethyl phosphate (0.36 mL, 2.099 mmol, 2.02 equiv.) were placed in a round flask and stirred at 110 ℃ for 32.0 h in an Ar atmosphere. After that, the excessive triethyl phosphate was evaporated under a reduced pressure. The

crude product was purified by column chromatography with petroleum ether/ethyl acetate (1/1, v/v) as eluent to obtain product as a pale yellow oil (418.6 mg, 82.45%). ^{1}H NMR (400 MHz, $CDCl_3$): δ (TMS, ppm) = 7.53 (d, J = 8.0 Hz, 2H), 7.40 (d, J = 8.0 Hz, 2H), 7.11 (d, J = 8.0 Hz, 2H), 7.07 (d, J = 8.0 Hz, 2H), 6.14–6.08 (m, 1H), 4.13–4.05 (m, 4H), 2.68 (d, J = 8.0 Hz, 1H), 2.63 (d, J = 8.0 Hz, 1H), 1.31 (t, J = 8.0 Hz, 6H). ^{13}C NMR (125 MHz, $CDCl_3$): δ (ppm) = 143.44 (d, J = 15.0 Hz), 140.33 (d, J = 2.5 Hz), 137.29 (d, J = 2.5 Hz), 131.69, 131.55, 131.46, 131.31, 128.89, 121.79 (d, J = 16.3 Hz), 118.66 (d, J = 11.3 Hz), 61.94 (d, J = 6.3 Hz), 28.43 (d, J = 140.0 Hz), 16.42 (d, J = 6.3 Hz). ^{31}P NMR (162 MHz, $CDCl_3$): δ (ppm) = 23.17. HRMS (ESI) m/z: $[M + H]^+$ Calcd for $C_{19}H_{22}Br_2O_3P$: 486.9668; Found: 486.9667.

(4) Synthesis of **4**

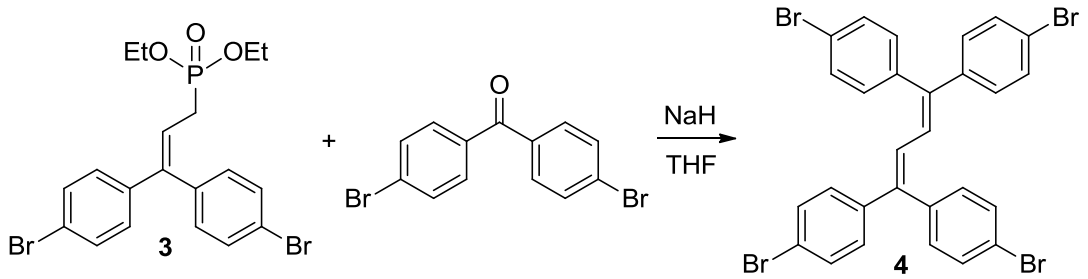

3 (3048.6 mg, 6.245 mmol, 1.00 equiv.), 4,4′-dibromobenzophenone (2336.5 mg, 6.872 mmol, 1.10 equiv.), sodium hydride (60% dispersion in mineral oil, 759.3 mg, 18.983 mmol, 3.04 equiv.), and THF (16 mL) were placed in a round flask and stirred at room temperature for 51.5 h in an Ar atmosphere. After that, the solvent was evaporated under a reduced pressure. The crude product was purified by column chromatography with petroleum ether/DCM (10/1, v/v) as eluent to obtain product as a yellow solid (4111.0 mg, 97.66%). ^{1}H NMR (400 MHz, $CDCl_3$): δ (TMS, ppm) = 7.55 (d, J = 8.0 Hz, 4H), 7.37 (d, J = 8.0 Hz, 4H), 7.14 (d, J = 8.0 Hz, 4H), 7.00 (d, J = 8.0 Hz, 4H), 6.65 (s, 2H). ^{13}C NMR (100 MHz, $CDCl_3$): δ (ppm) = 142.72, 140.60, 137.95, 132.17, 131.68, 131.47, 129.21, 126.04, 122.16, 122.03. CCDC: 1997188.

(5) Synthesis of **5**–**7**

5–**7** were synthesized according to our previous procedures.[5]

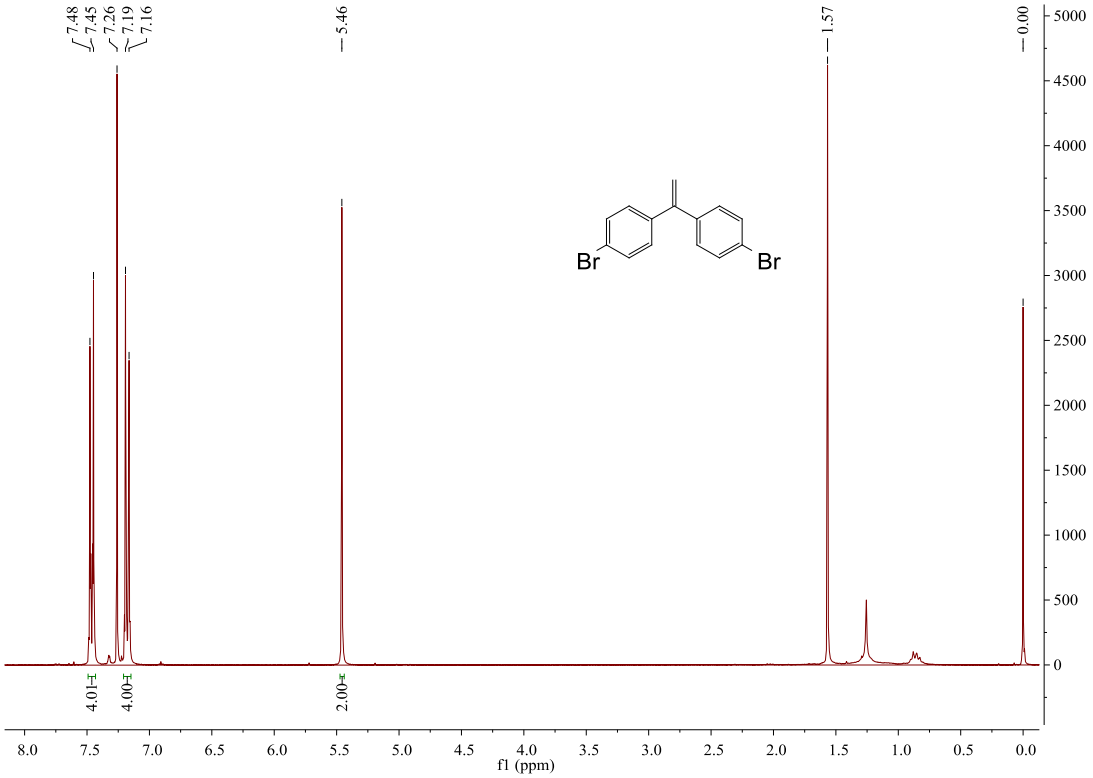

Figure S1. ^{1}H NMR spectrum of **1** (300 MHz, $CDCl_3$).

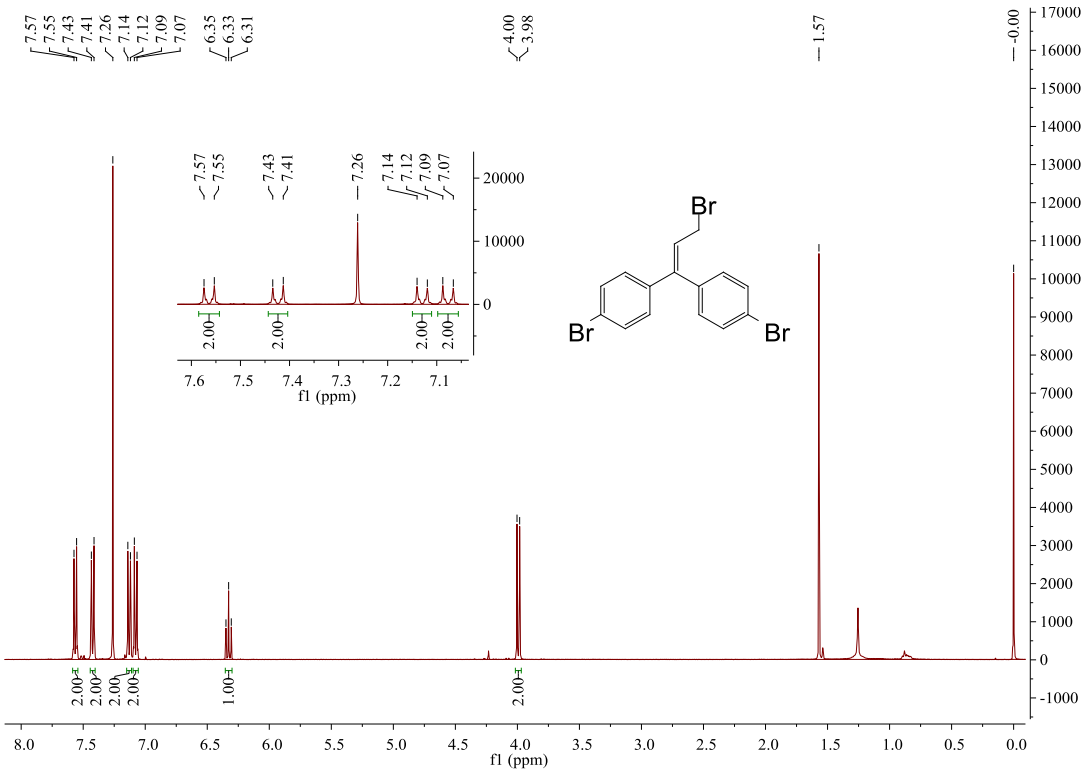

Figure S2. ^{1}H NMR spectrum of **2** (400 MHz, $CDCl_3$).

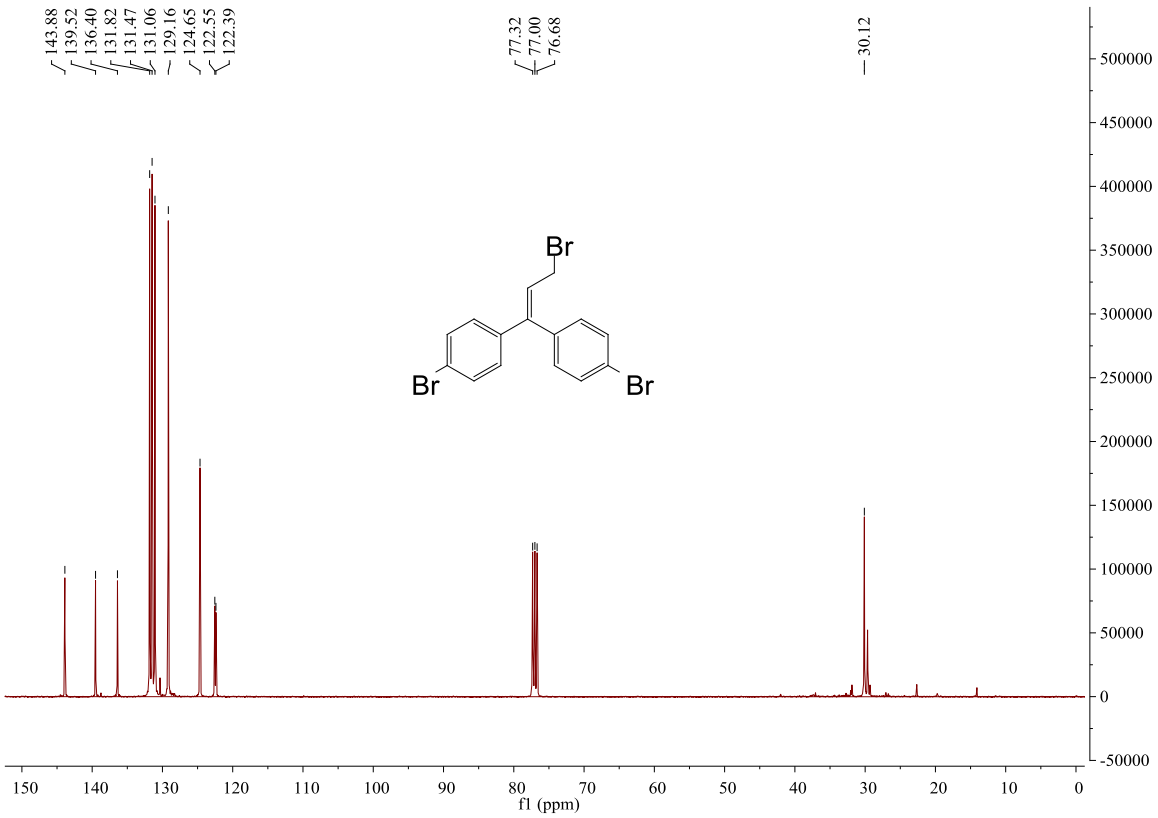

Figure S3. ^{13}C NMR spectrum of **2** (100 MHz, $CDCl_3$).

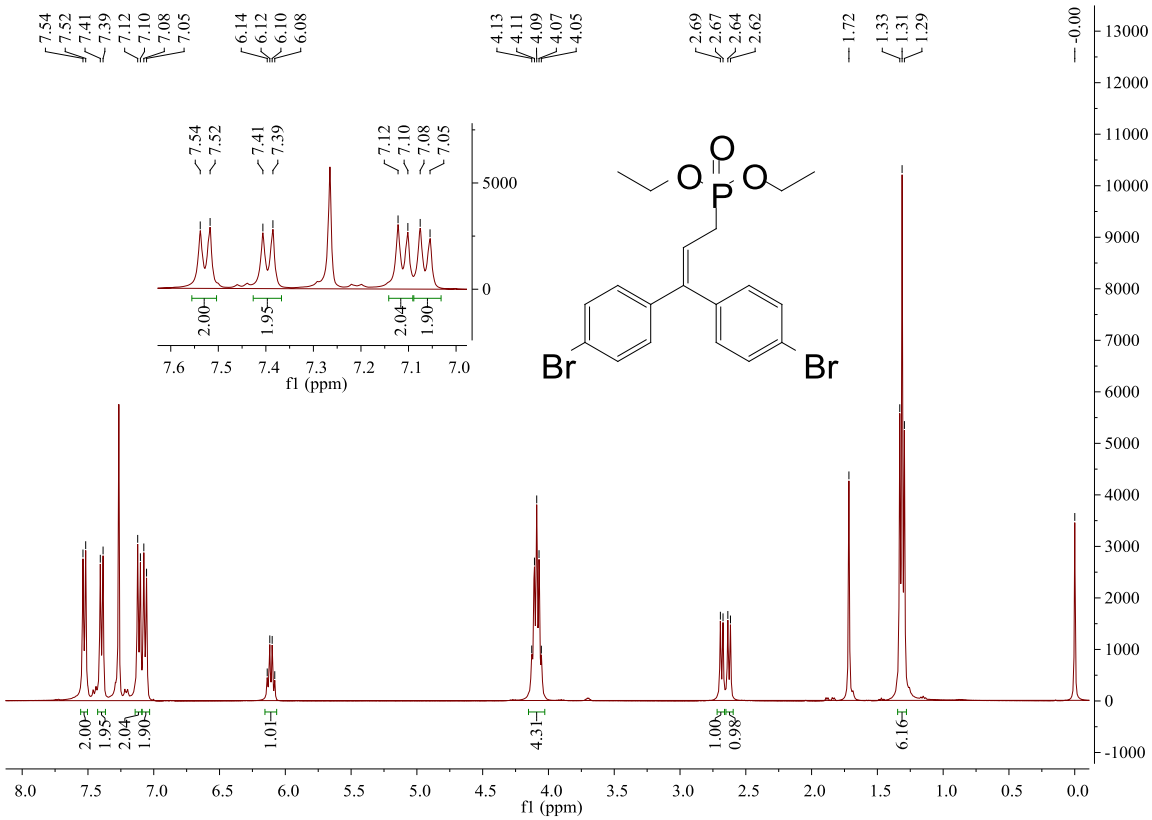

Figure S4. ^{1}H NMR spectrum of **3** (400 MHz, $CDCl_3$).

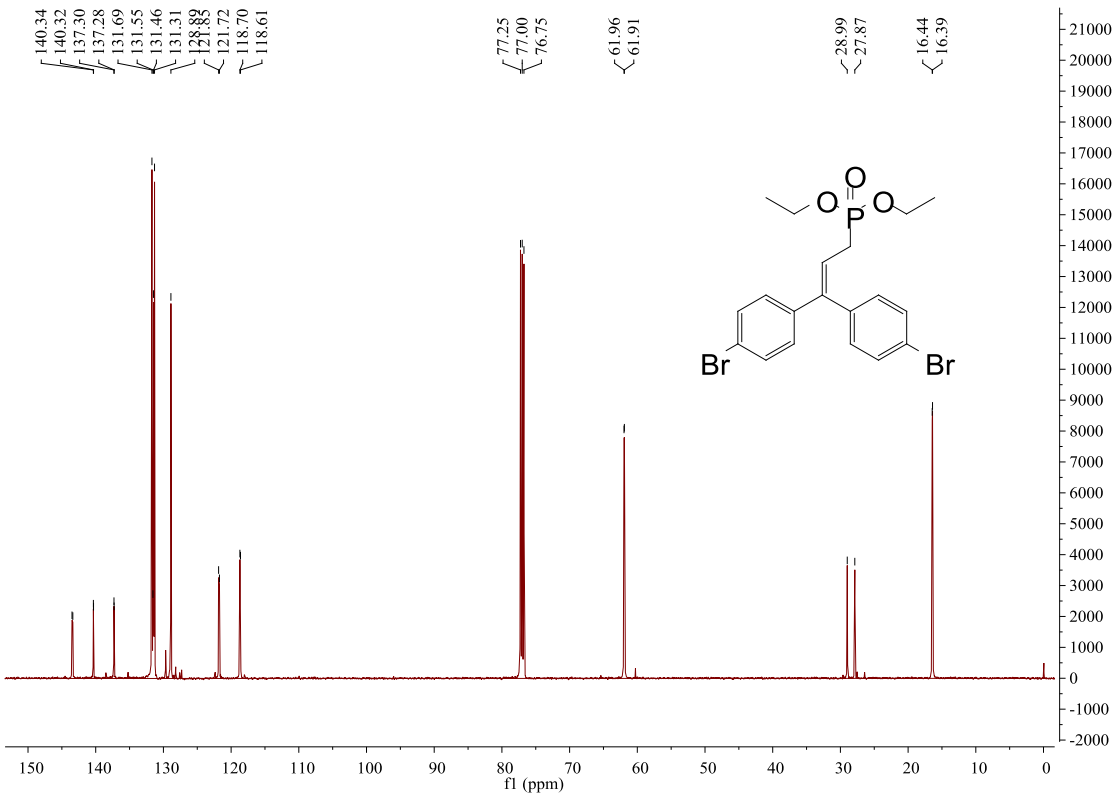

Figure S5. ^{13}C NMR spectrum of **3** (125 MHz, $CDCl_3$).

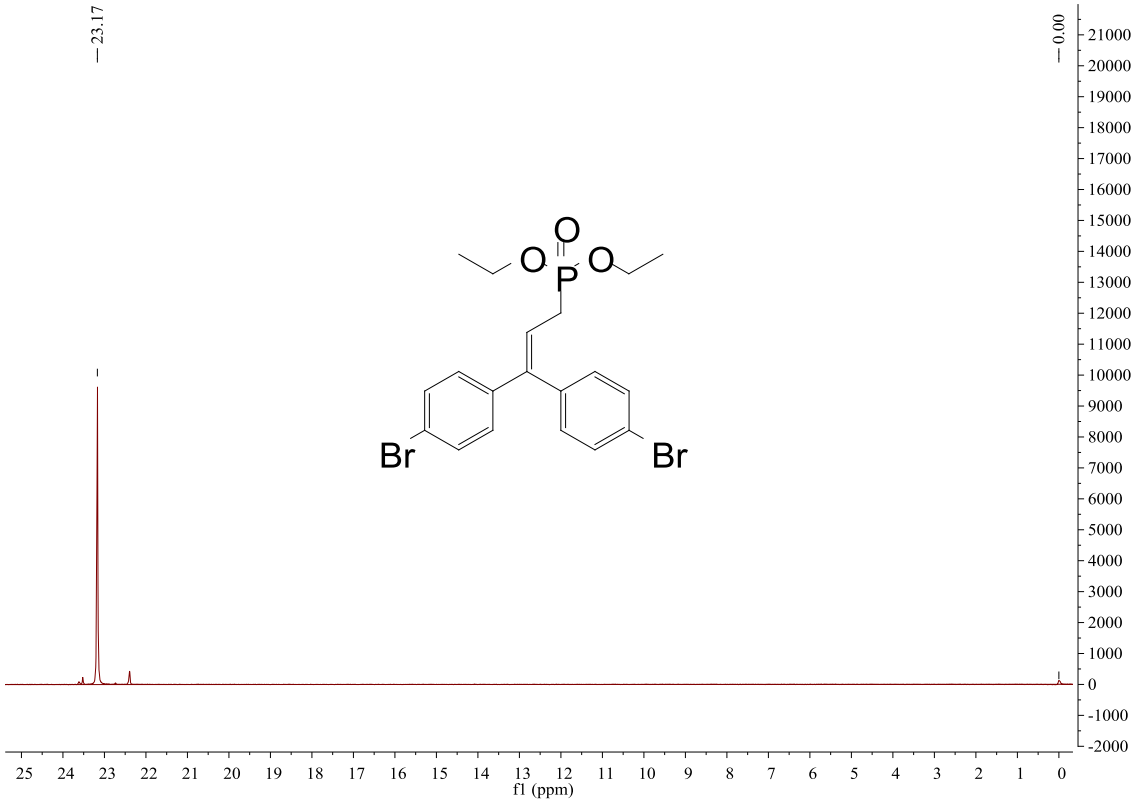

Figure S6. ^{31}P NMR spectrum of **3** (162 MHz, $CDCl_3$).

Display Report

Analysis Info

Analysis Name	D:\Data\Shao Guang\MS\lisuanzhi1.d	Acquisition Date	5/10/2017 4:24:05 PM	
Method	tune_mid_ESI+.m	Operator	BDAL@DE	
Sample Name	lisuanzhi1	Instrument	maXis 4G	21242
Comment				

Acquisition Parameter

Source Type	ESI	Ion Polarity	Positive	Set Nebulizer	0.4 Bar
Focus	Active	Set Capillary	4500 V	Set Dry Heater	180 °C
Scan Begin	100 m/z	Set End Plate Offset	-500 V	Set Dry Gas	4.0 l/min
Scan End	2900 m/z	Set Collision Cell RF	1500.0 Vpp	Set Divert Valve	Source

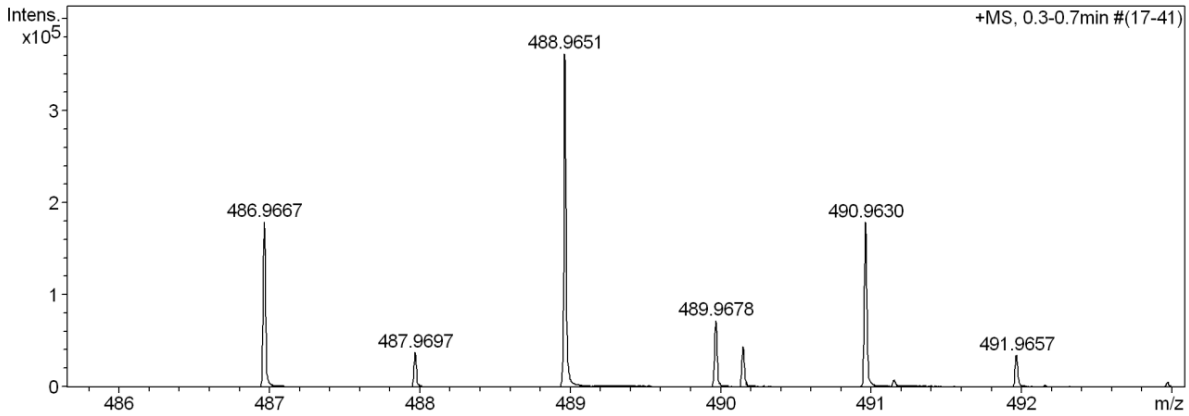

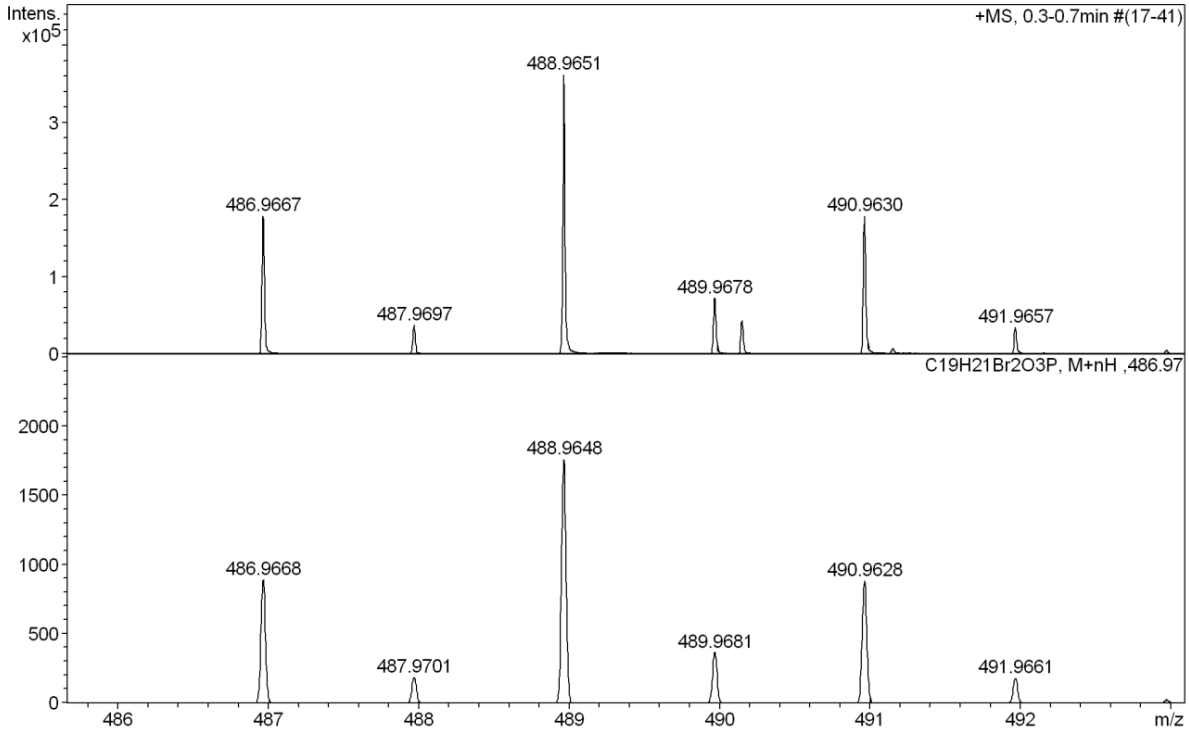

Bruker Compass DataAnalysis 4.0 printed: 5/10/2017 5:05:37 PM Page 1 of 1

Figure S7. HRMS spectrum of **3**.

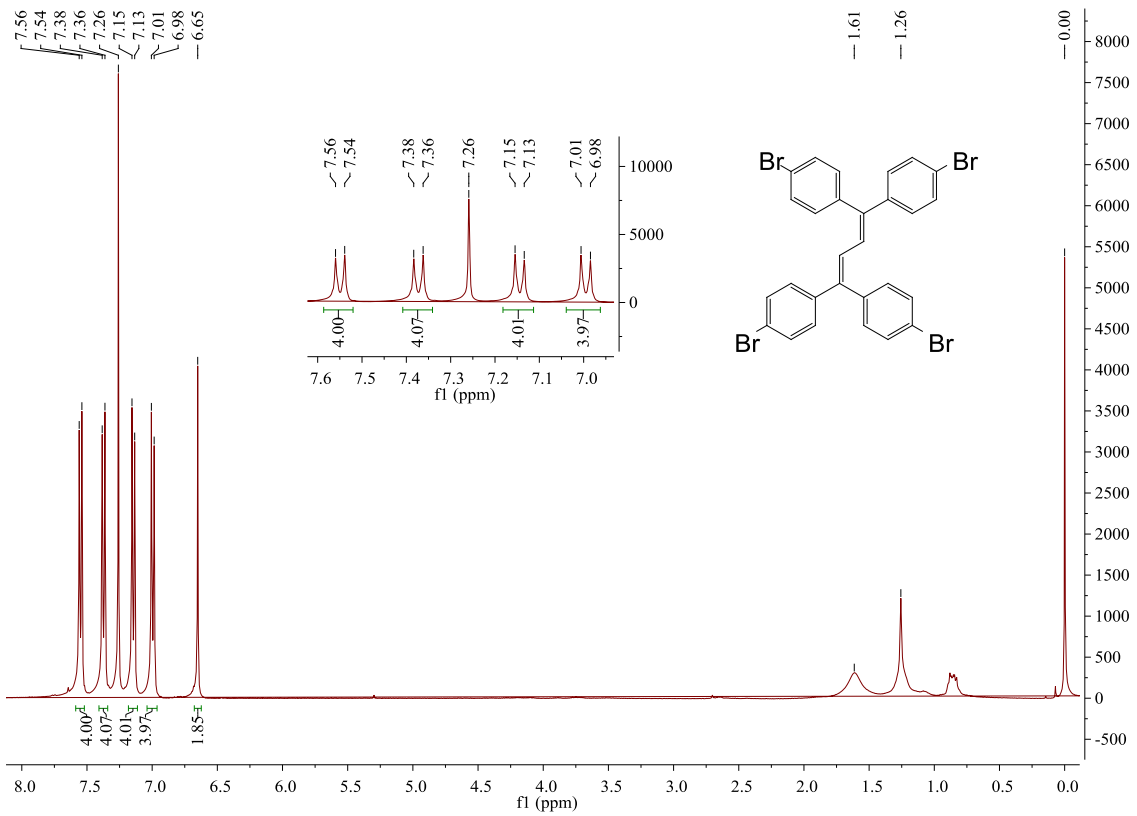

Figure S8. ^{1}H NMR spectrum of **4** (400 MHz, $CDCl_3$).

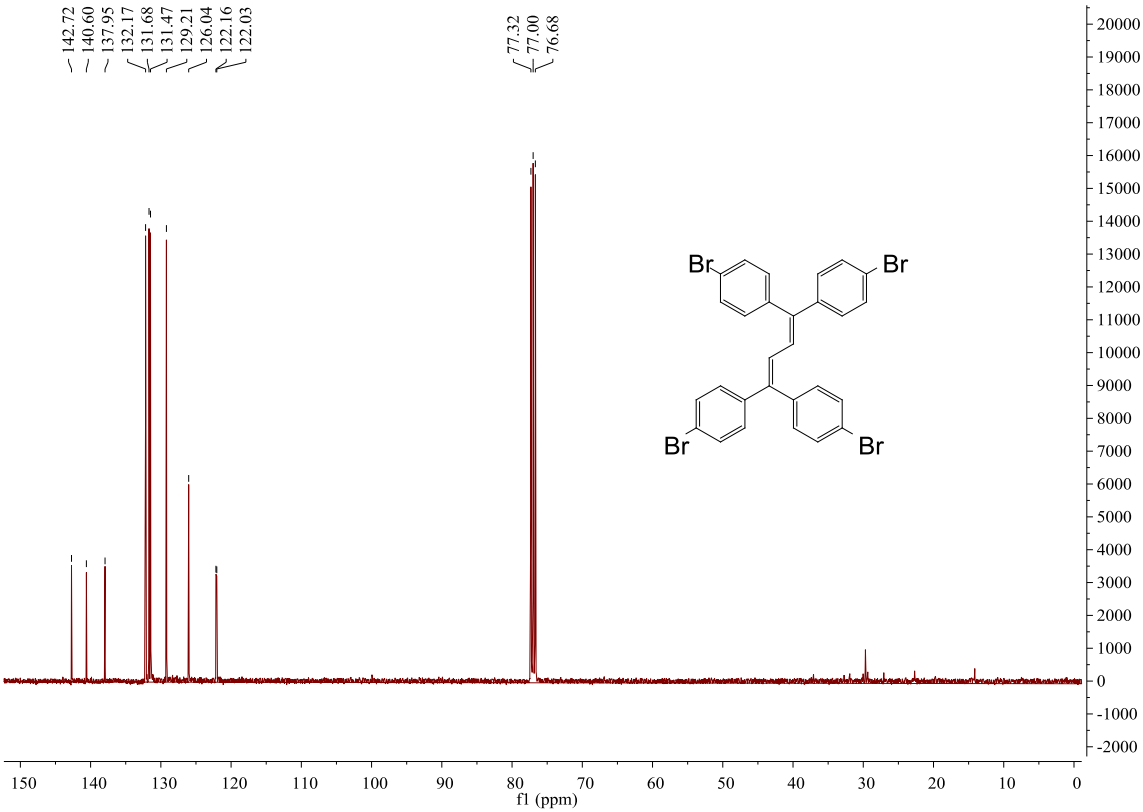

Figure S9. ^{13}C NMR spectrum of **4** (100 MHz, $CDCl_3$).

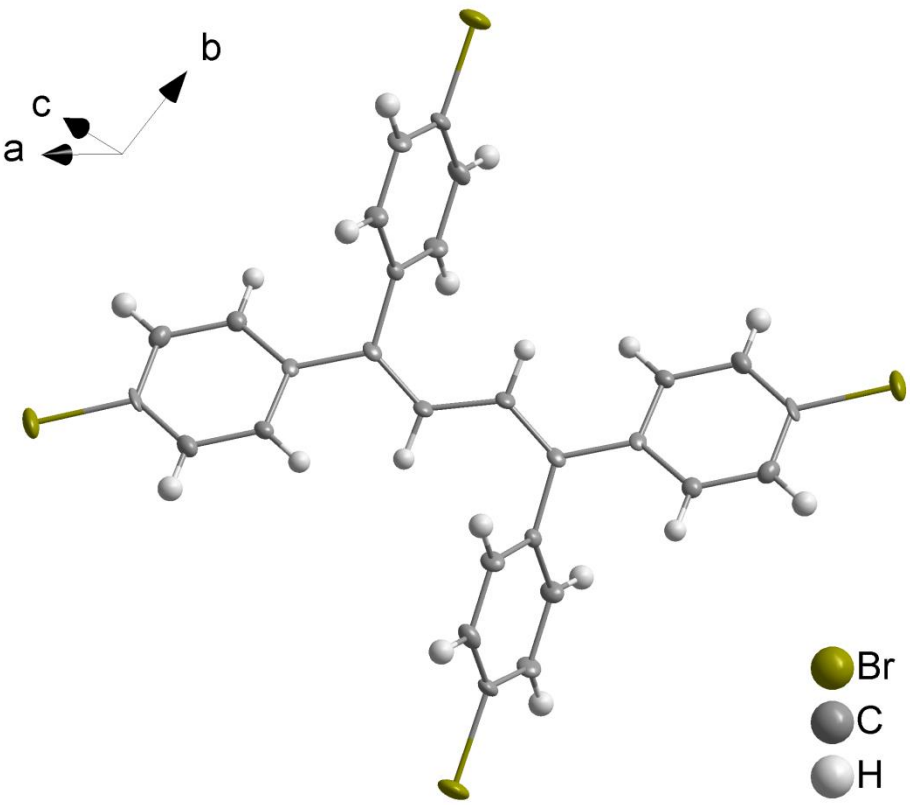

Figure S10. ORTEP representation of **4** (50% probability thermal ellipsoids; solvents were omitted for clarity).

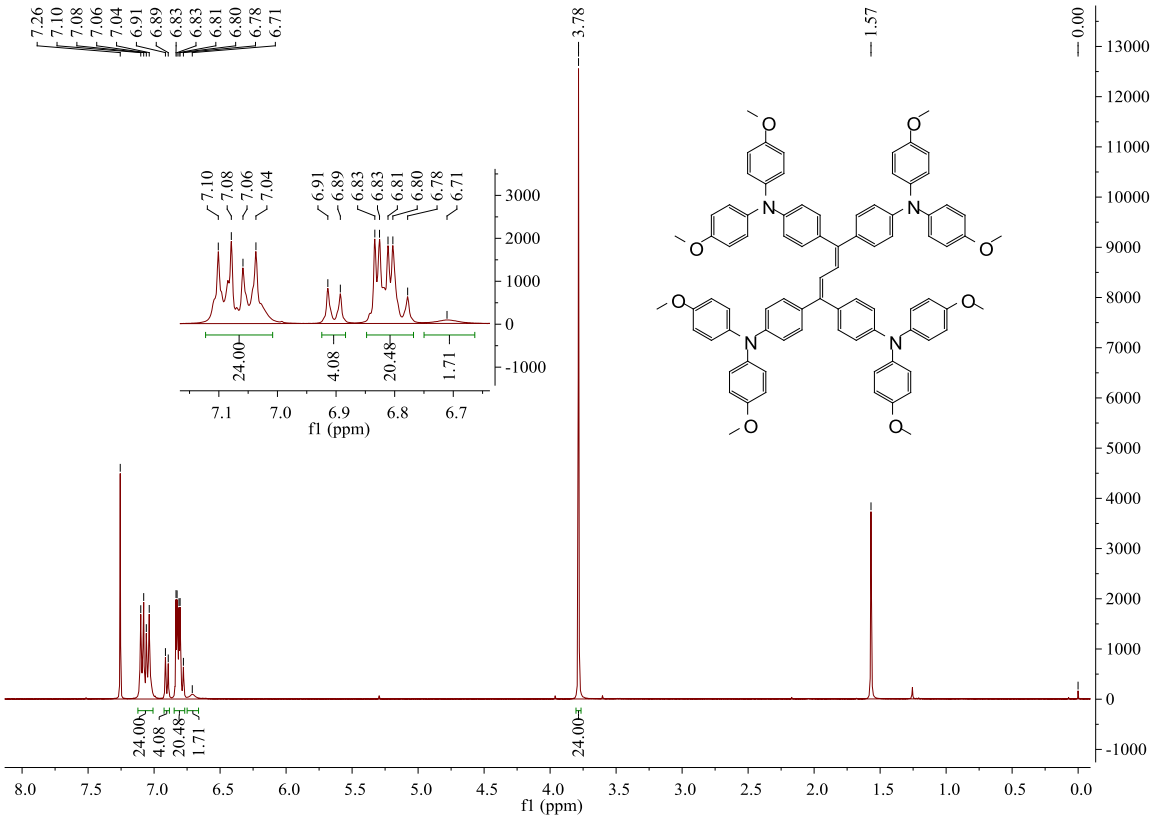

Figure S11. ^{1}H NMR spectrum of **CJ-03** (400 MHz, $CDCl_3$).

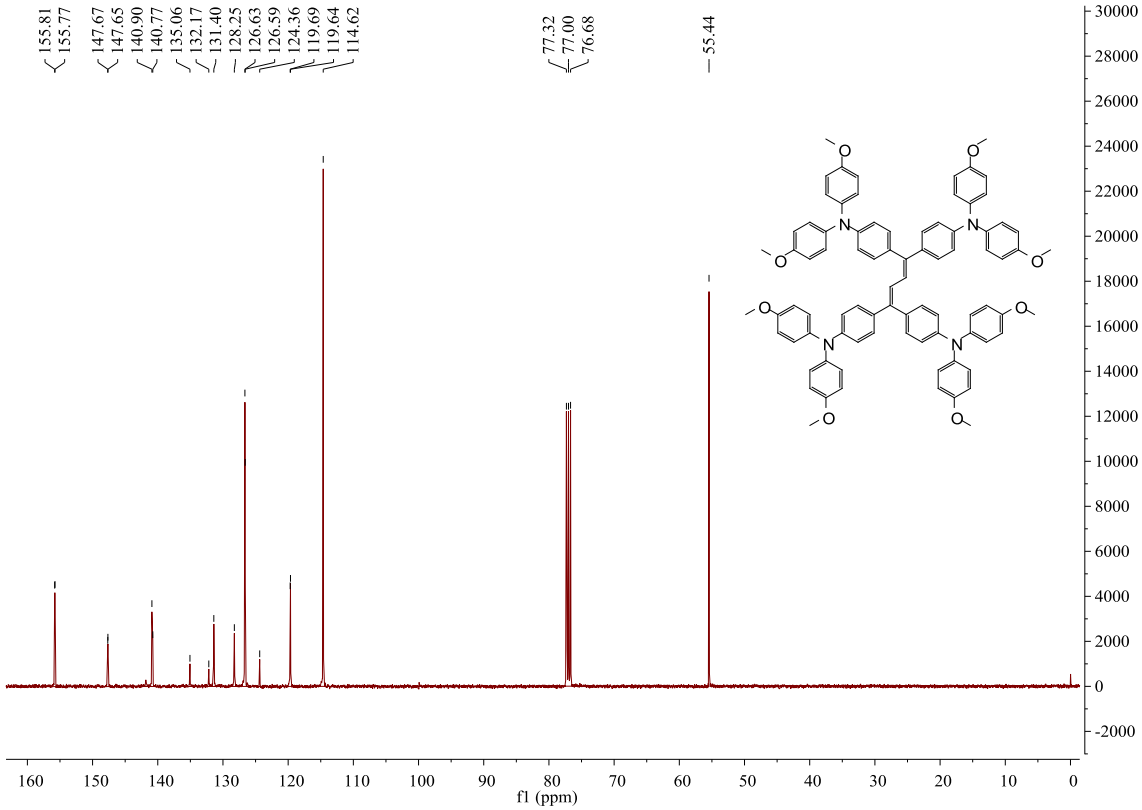

Figure S12. ^{13}C NMR spectrum of **CJ-03** (100 MHz, $CDCl_3$).

Display Report

Analysis Info

Analysis Name	D:\Data\shaoguang\chenjian\20180108-R716-acetone.d	Acquisition Date	1/8/2018 12:11:15 PM
Method	tune_mid_ESI+.m	Operator	BDAL@DE
Sample Name	20180108-R716-acetone	Instrument	maXis 4G 21242
Comment			

Acquisition Parameter

Source Type	ESI	Ion Polarity	Positive	Set Nebulizer	0.4 Bar
Focus	Active	Set Capillary	3500 V	Set Dry Heater	180 °C
Scan Begin	100 m/z	Set End Plate Offset	-500 V	Set Dry Gas	4.0 l/min
Scan End	2800 m/z	Set Collision Cell RF	1500.0 Vpp	Set Divert Valve	Source

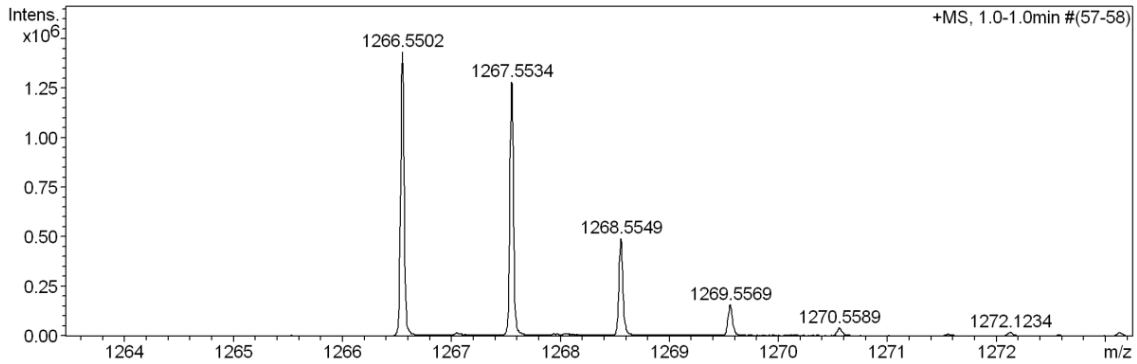

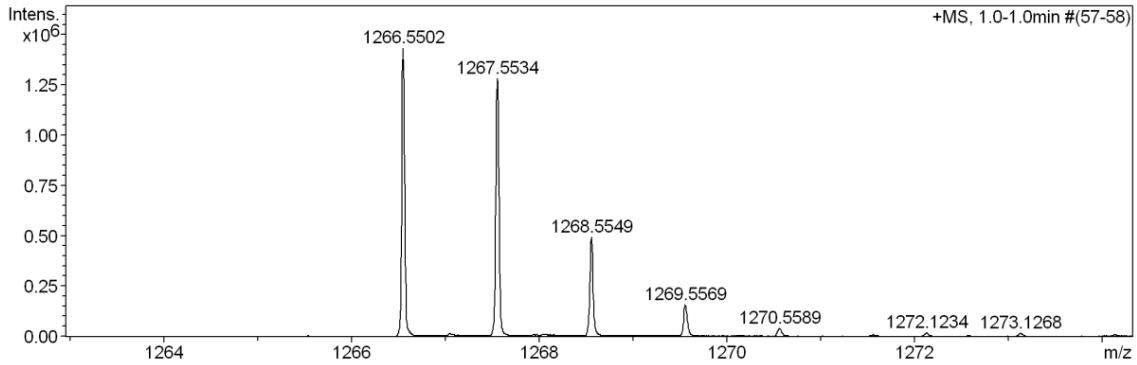

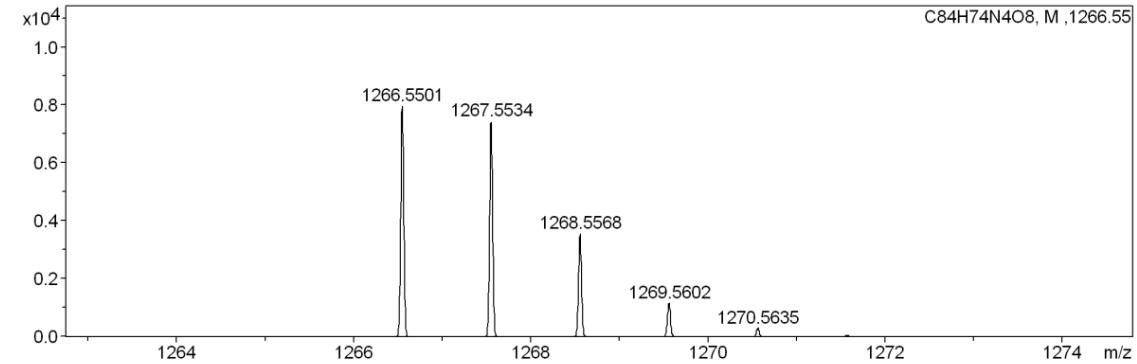

Bruker Compass DataAnalysis 4.0 printed: 1/8/2018 12:17:04 PM Page 1 of 1

Figure S13. HRMS spectrum of **CJ-03**.

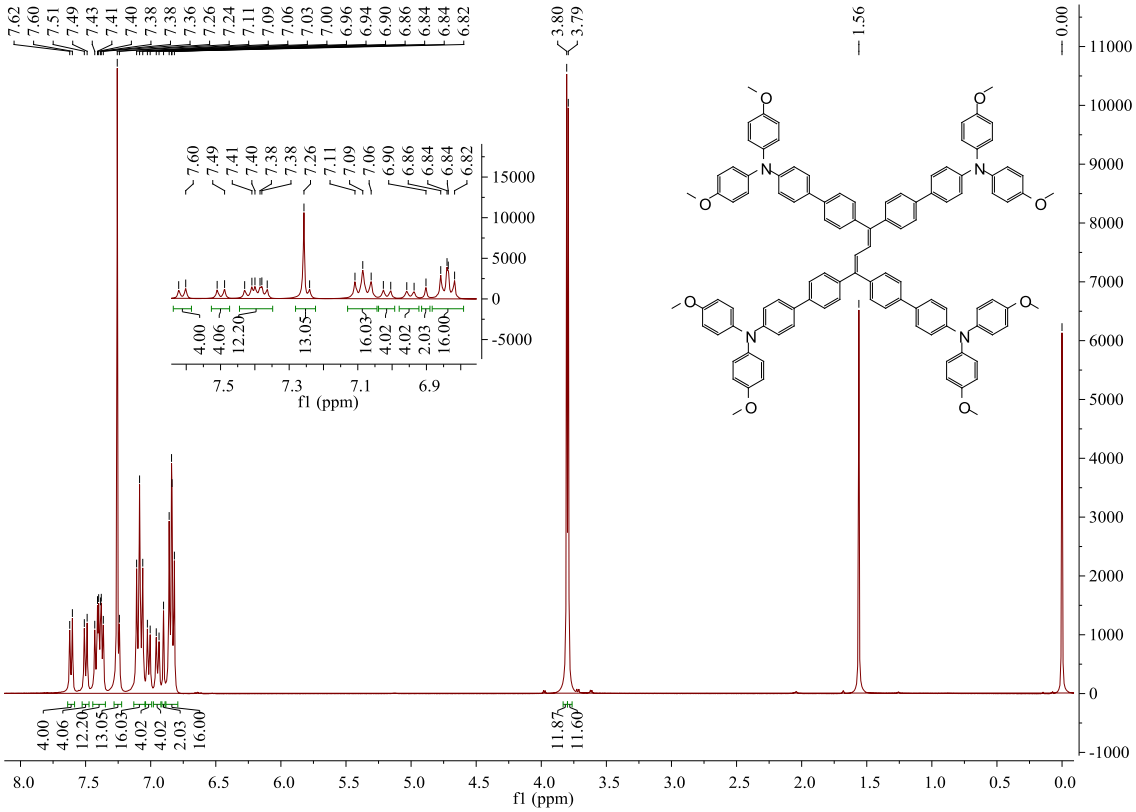

Figure S14. ^{1}H NMR spectrum of **CJ-04** (400 MHz, $CDCl_3$).

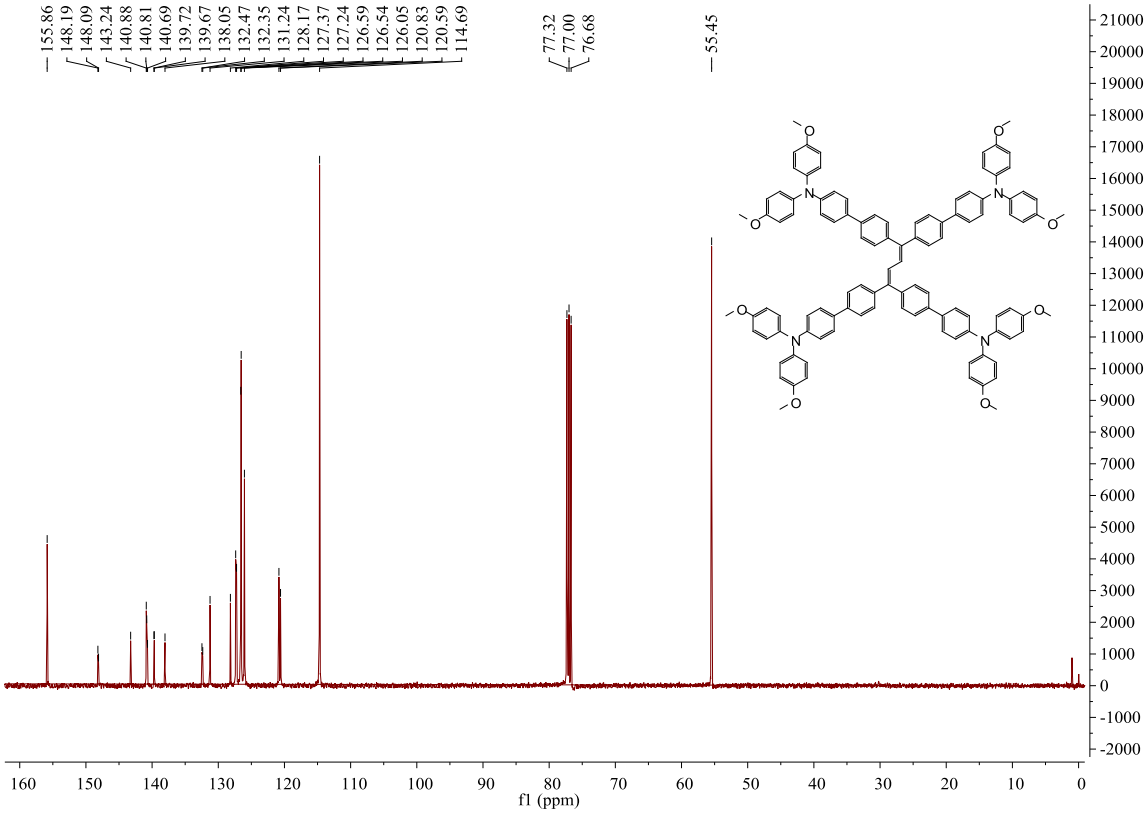

Figure S15. ^{13}C NMR spectrum of **CJ-04** (100 MHz, $CDCl_3$).

Display Report

Analysis Info

Analysis Name	D:\Data\shaoguang\chenjian\20171214-R453-CHCl3-CH3CN.d	Acquisition Date	12/14/2017 9:26:28 PM	
Method	tune_mid.m	Operator	BDAL@DE	
Sample Name	20171214-R453-CHCl3-CH3CN	Instrument	maXis 4G	21242
Comment				

Acquisition Parameter

Source Type	ESI	Ion Polarity	Positive	Set Nebulizer	0.4 Bar
Focus	Active	Set Capillary	4500 V	Set Dry Heater	180 °C
Scan Begin	100 m/z	Set End Plate Offset	-500 V	Set Dry Gas	4.0 l/min
Scan End	2900 m/z	Set Collision Cell RF	1500.0 Vpp	Set Divert Valve	Waste

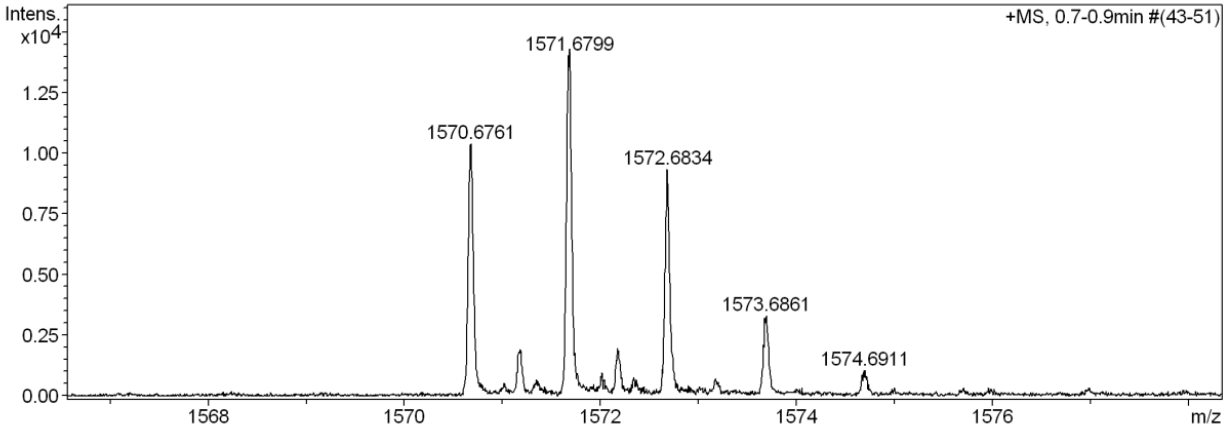

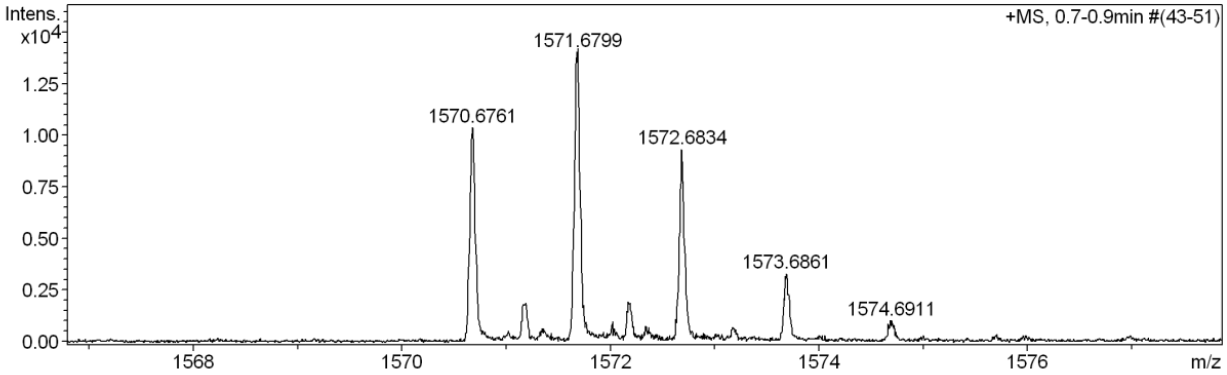

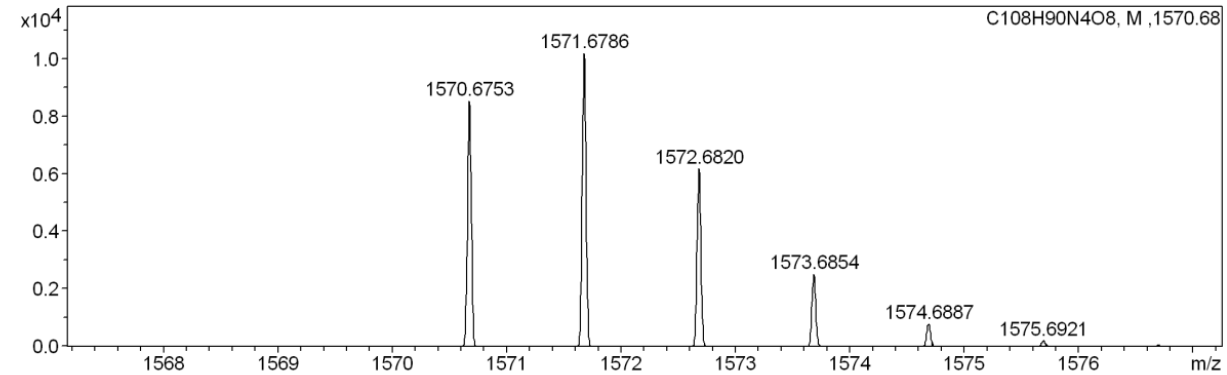

Bruker Compass DataAnalysis 4.0 printed: 12/14/2017 9:36:10 PM Page 1 of 1

Figure S16. HRMS spectrum of **CJ-04**.

3. Computational study

Table S1. Optimized molecular configuration, HOMOs, and LUMOs of HTMs obtained from DFT calculations

HTM	Optimized molecular configuration	HOMO	LUMO
CJ-03	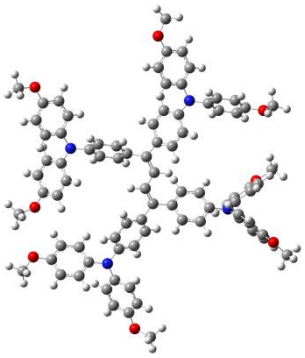	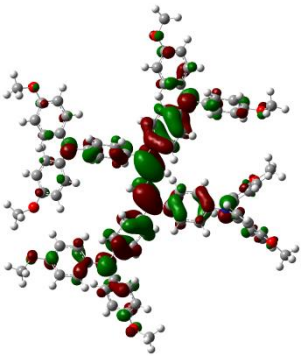	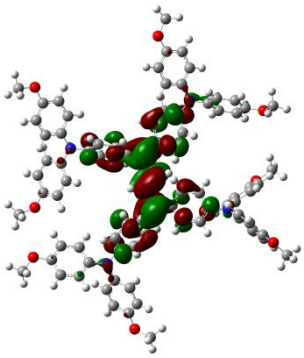
CJ-04	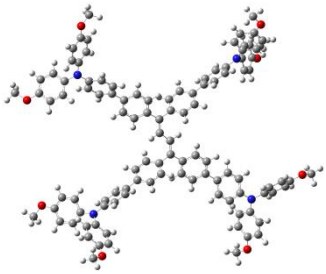	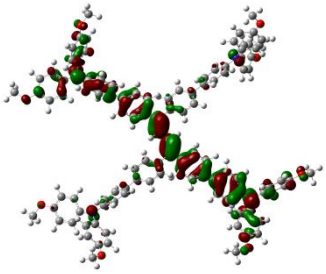	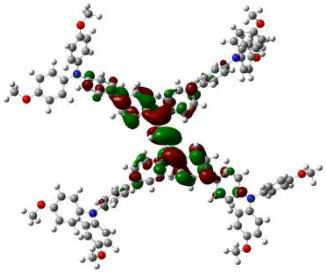
spiro-OMeTAD	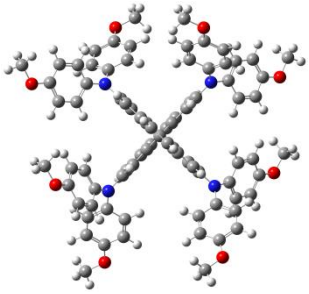	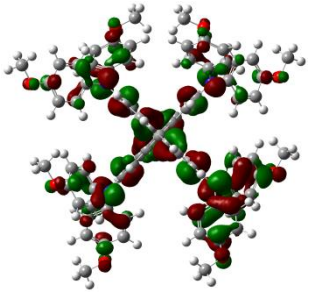	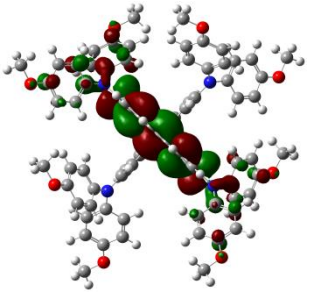

Table S2. Theoretical energy levels of HTMs

HTM	E_{HOMO} (eV)	E_{LUMO} (eV)	E_{gap} (eV)
CJ-03	–4.16	–1.27	2.89
CJ-04	–4.44	–1.54	2.90
spiro-OMeTAD	–4.33	–0.71	3.62

Table S3 Electrostatic surface potential (ESP) map and dipole moment of HTMs

HTM	Dipole moment (Debye, D)	ESP
CJ-03	4.71	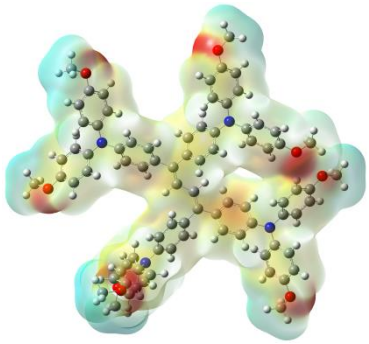
CJ-04	5.06	
spiro-OMeTAD	6.19	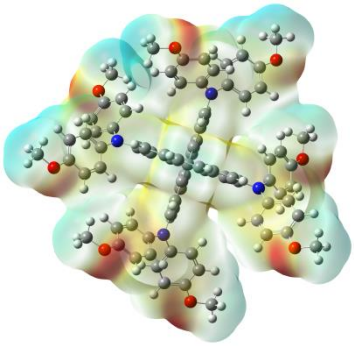

4. Aggregation-induced emission

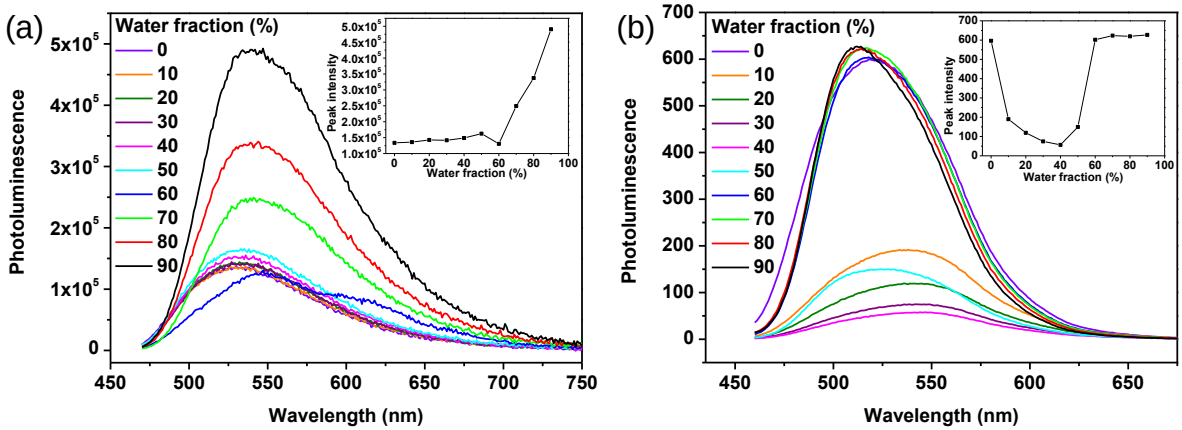

Figure S17. PL spectra of (a) **CJ-03** and (b) **CJ-04** in water/THF mixtures with various volume fractions of water (1.0×10^{-5} M). The insets portray the changes in PL maximum intensity.

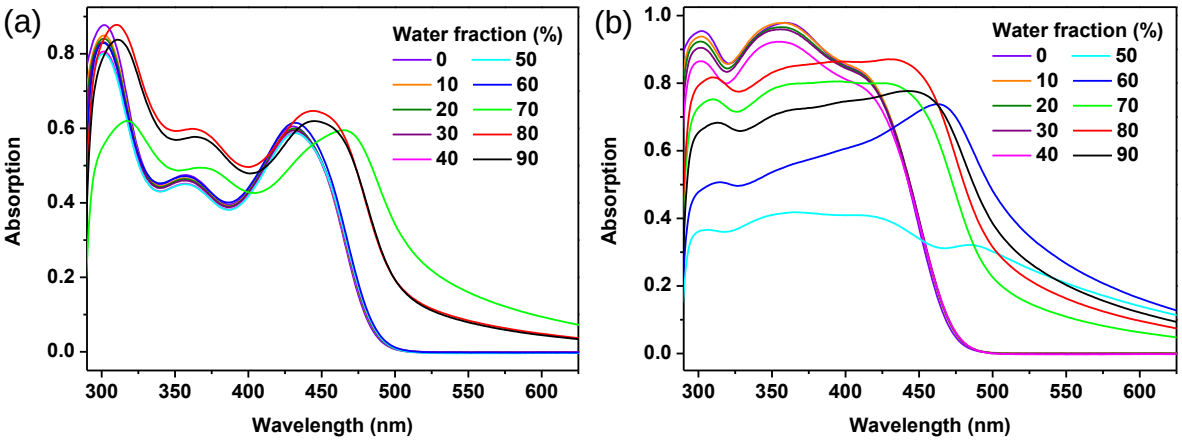

Figure S18. UV–vis absorption spectra of (a) **CJ-03** and (b) **CJ-04** in water/THF mixtures with various volume fractions of water (1.0×10^{-5} M).

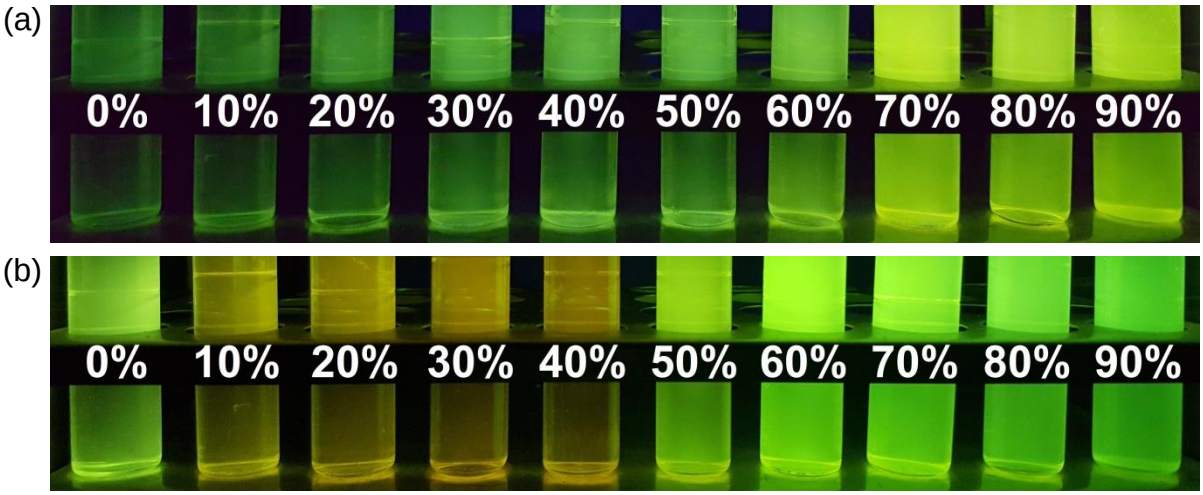

Figure S19. Picture of (a) **CJ-03** and (b) **CJ-04** in water/THF mixtures with various volume fractions of water (1.0×10^{-5} M) irradiated by UV light (365 nm).

Table S4. Photophysical parameters of **CJ-03** in water/THF mixtures with various volume fractions of water (1.0×10^{-5} M)

Water fraction (%)	λ_{abs} (nm)	ε (M^{-1} cm^{-1})	λ_{ex} (nm)	λ_{em} (nm)
0	430	60505	450	531
10	431	59859	450	533
20	431	59915	450	534
30	431	59444	450	534
40	431	58762	450	535
50	432	58678	450	536
60	431	61497	450	547
70	465	59498	450	541
80	444	64680	450	540
90	445	61953	449	540

Table S5. Photophysical parameters of **CJ-04** in water/THF mixtures with various volume fractions of water (1.0×10^{-5} M)

Water fraction (%)	λ_{abs} (nm)	ε (M^{-1} cm^{-1})	λ_{ex} (nm)	λ_{em} (nm)
0	359	97884	437	521
10	357	97846	438	537
20	356	96572	438	541
30	355	95926	442	543
40	353	92246	441	543
50	364	41834	453	528
60	463	73790	449	519
70	428	79950	450	516
80	434	86984	449	515
90	443	77691	450	512

5. Thermal behaviors

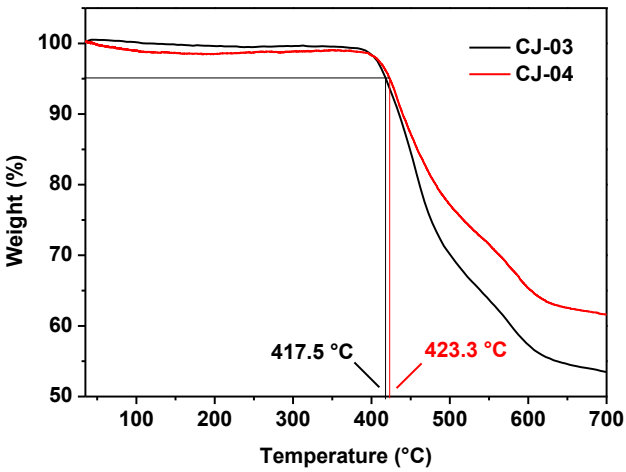

Figure S20. TGA of HTMs (10 K/min, N_2 atmosphere).

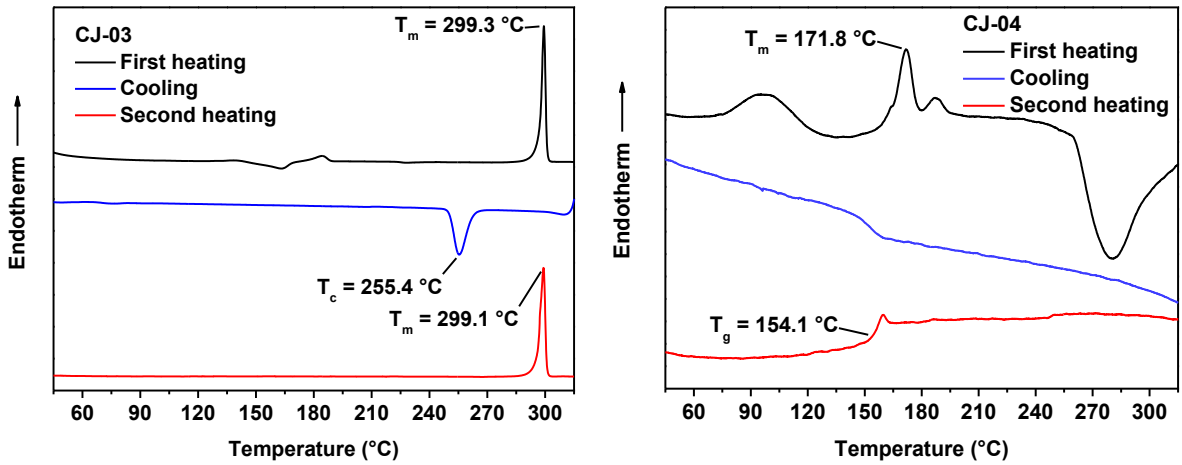

Figure S21. DSC of HTMs (10 K/min, N_2 atmosphere).

6. Photophysical properties

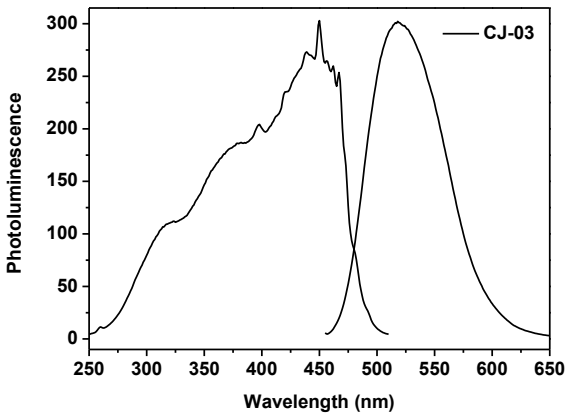

Figure S22. PL spectra of **CJ-03** (1.0×10^{-5} M in DCM; λ_{ex} = 450 nm, λ_{em} = 518 nm; slit: 3.0 nm, 3.0 nm).

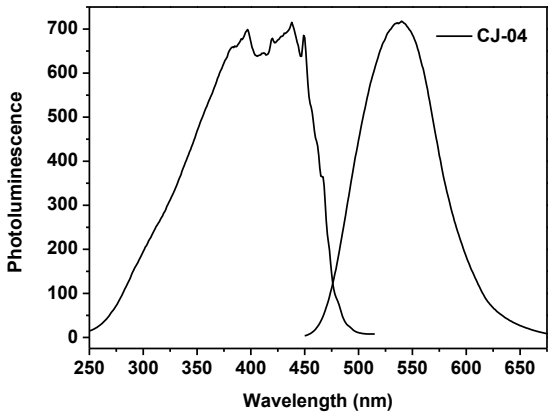

Figure S23. PL spectra of **CJ-04** (1.0×10^{-5} M in DCM; λ_{ex} = 438 nm, λ_{em} = 540 nm; slit: 3.0 nm, 3.0 nm).

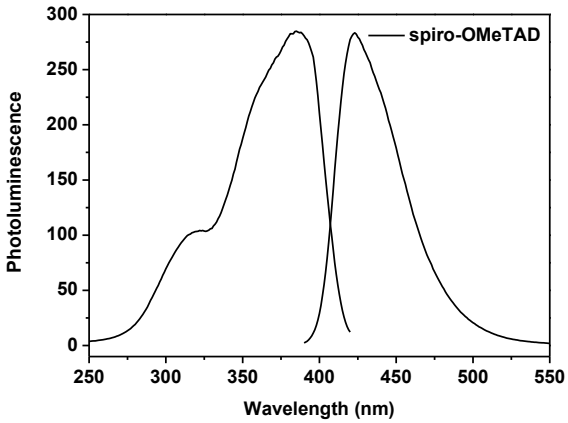

Figure S24. PL spectra of spiro-OMeTAD (1.0 × 10^{-5} M in DCM; λ_{ex} = 384 nm, λ_{em} = 423 nm; slit: 3.0 nm, 3.0 nm).

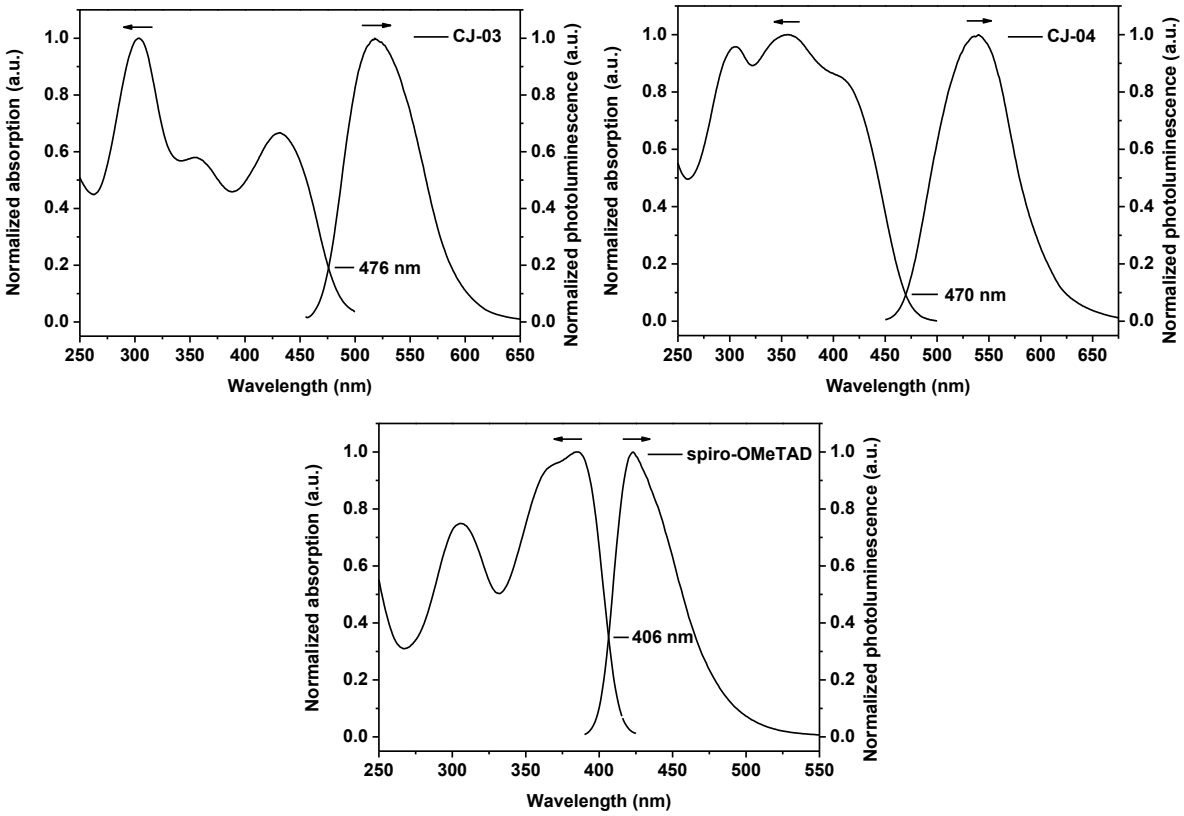

Figure S25. Normalized UV–vis absorption and emission spectra of HTMs (1.0 × 10^{-5} M in DCM).

7. Hole mobility measurements

Hole mobility of HTMs was evaluated using space-charge-limited current method according to our previous work.[5] The film thicknesses of **CJ-03**, **CJ-04**, and spiro-OMeTAD are 145, 133, and 190 nm, respectively.

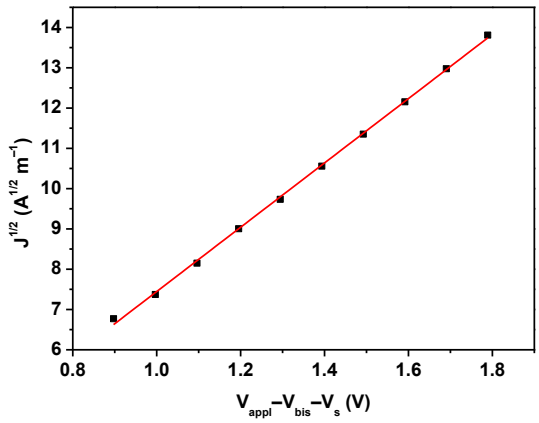

Figure S26. $J^{1/2}$–V characteristics of the hole-only device with **CJ-03**.

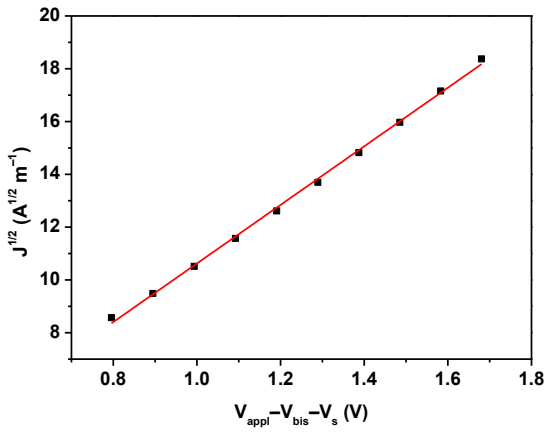

Figure S27. $J^{1/2}$–V characteristics of the hole-only device with **CJ-04**.

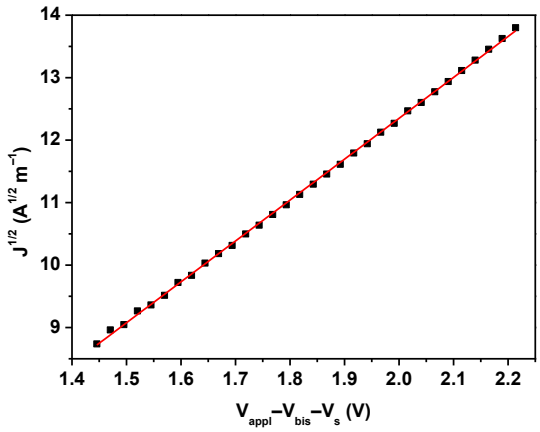

Figure S28. $J^{1/2}$–V characteristics of the hole-only device with spiro-OMeTAD.

8. Single-crystal crystallography

The methods for the collection of crystallography data, solution to the structure, and refinement of the structure were detailed in our early work.[5] The crystal structure of 1,1,2,2-tetrakis(4-bromophenyl)ethene was published by Tanaka *et al*.[6]

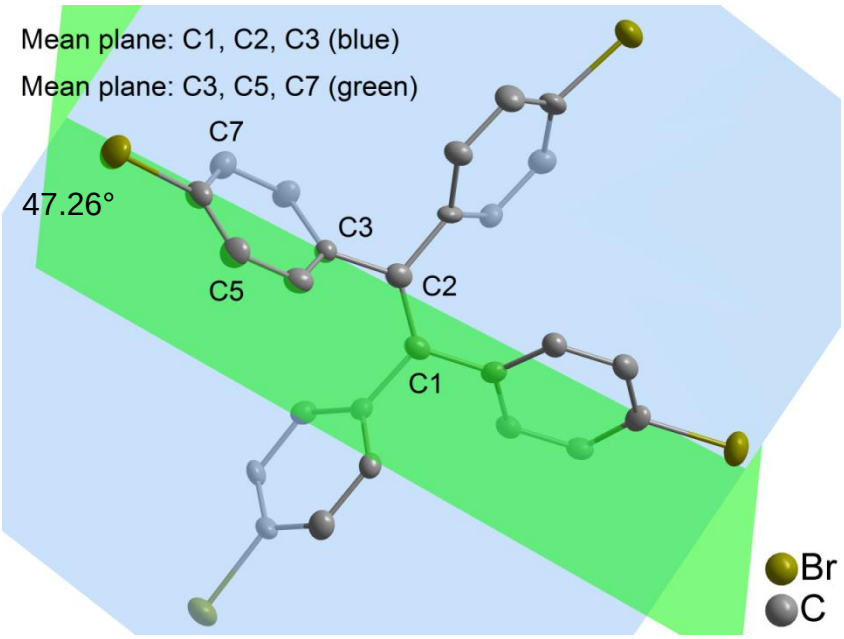

Figure S29. Dihedral angle between central ethylenic bond and surrounding phenyl ring (47.26°; solvents and H atoms were omitted for clarity).

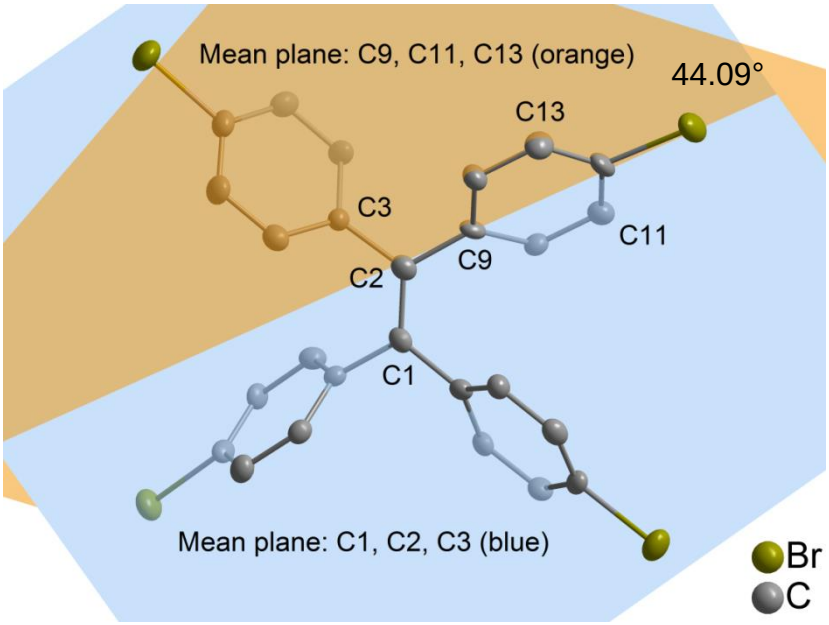

Figure S30. Dihedral angle between central ethylenic bond and surrounding phenyl ring (44.09°; solvents and H atoms were omitted for clarity).

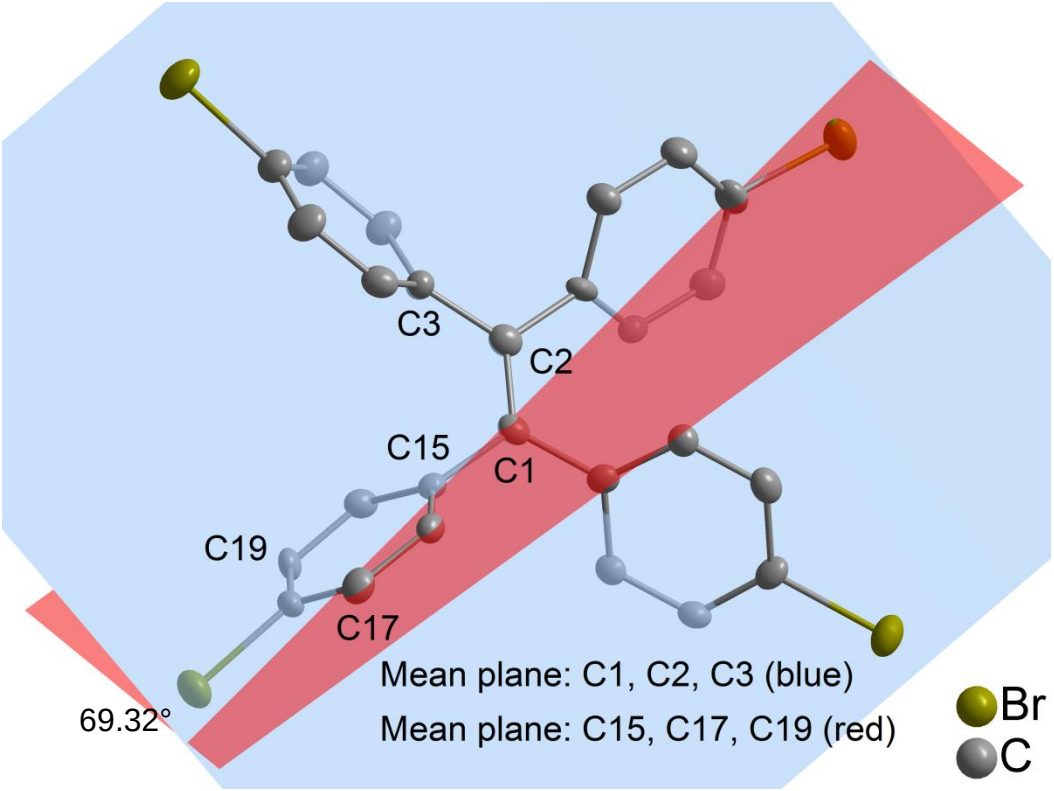

Figure S31. Dihedral angle between central ethylenic bond and surrounding phenyl ring (69.32 °; solvents and H atoms were omitted for clarity).

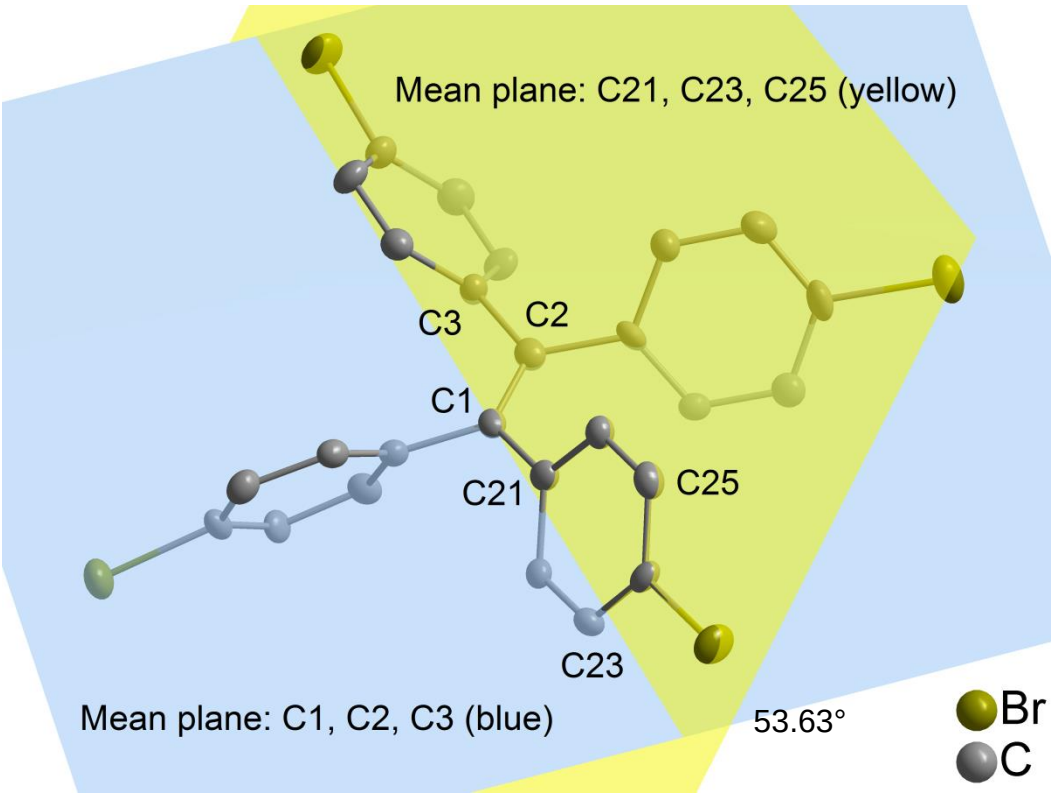

Figure S32. Dihedral angle between central ethylenic bond and surrounding phenyl ring (53.63 °; solvents and H atoms were omitted for clarity).

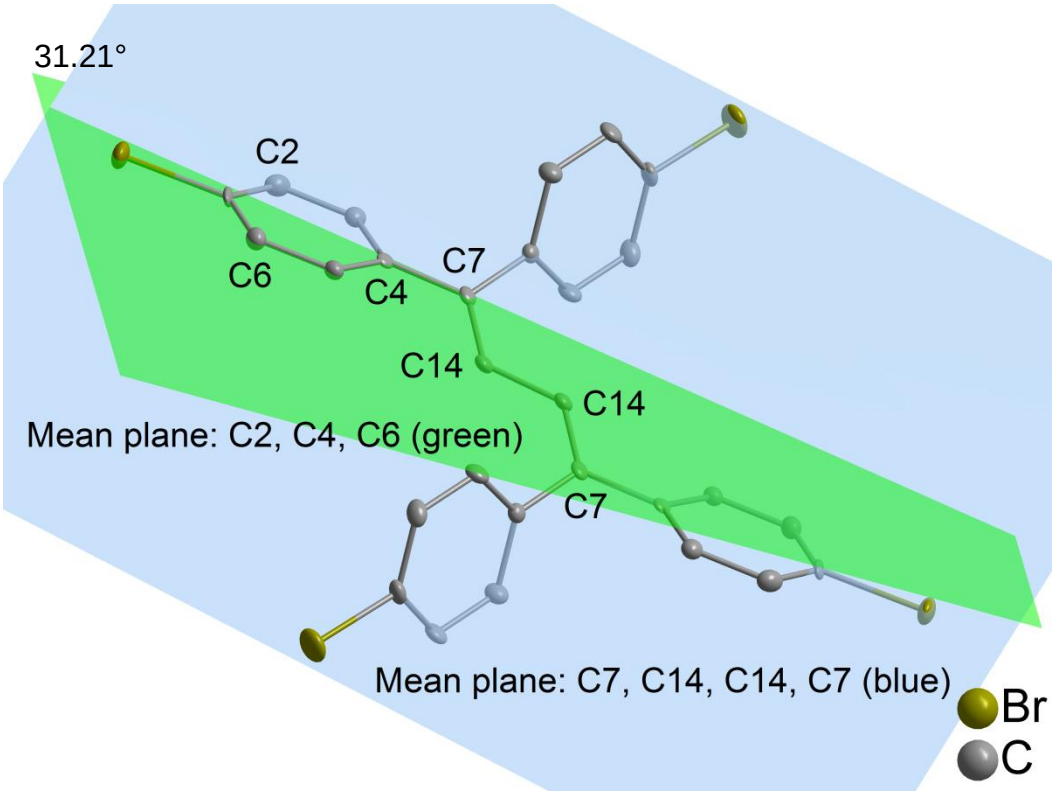

Figure S33. Dihedral angle between central butadiene and surrounding phenyl ring (31.21°; solvents and H atoms were omitted for clarity).

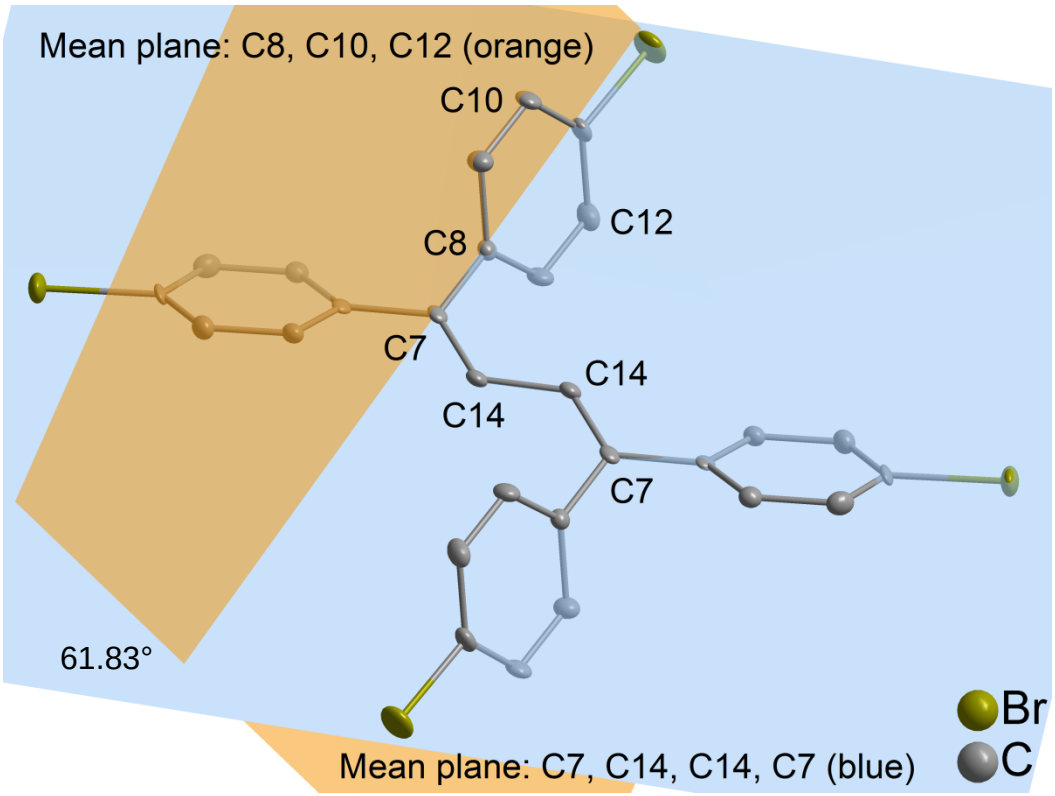

Figure S34. Dihedral angle between central butadiene and surrounding phenyl ring (61.83°; solvents and H atoms were omitted for clarity).

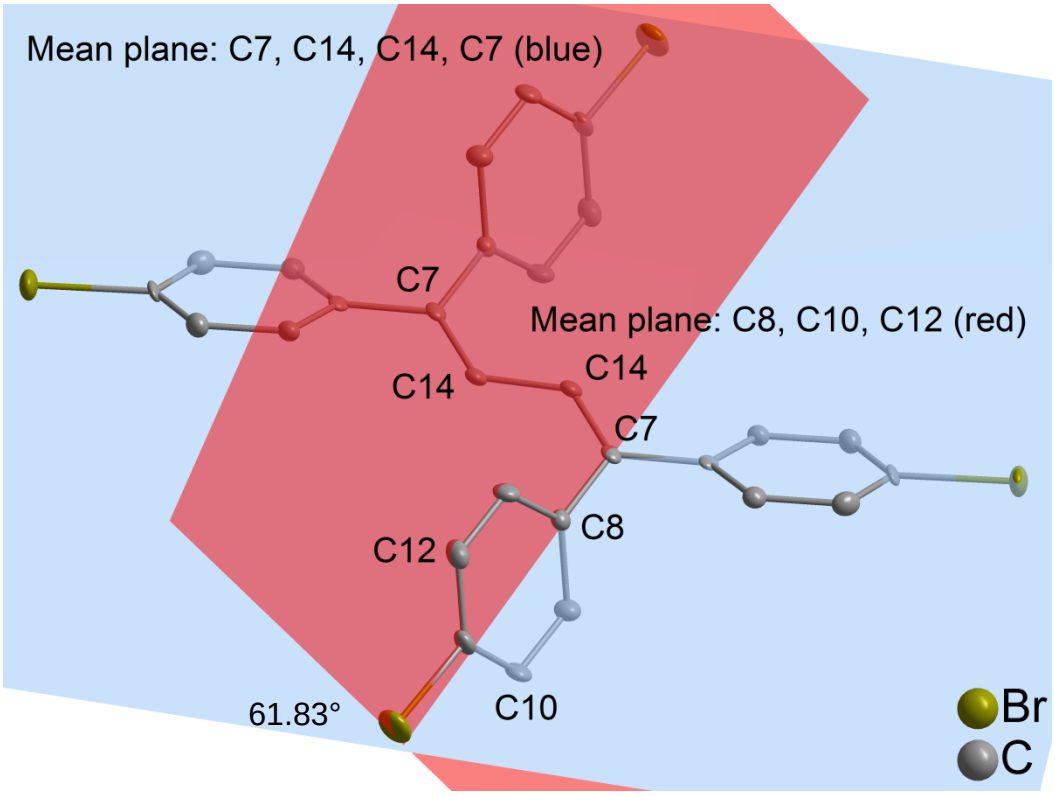

Figure S35. Dihedral angle between central butadiene and surrounding phenyl ring (61.83°; solvents and H atoms were omitted for clarity).

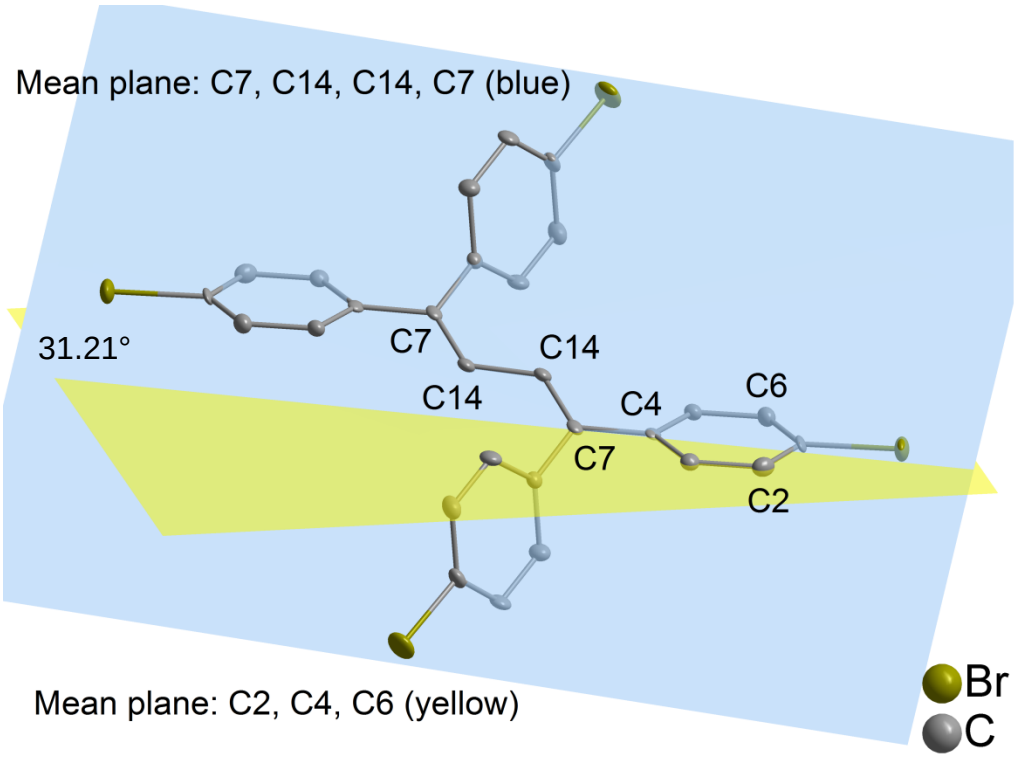

Figure S36. Dihedral angle between central butadiene and surrounding phenyl ring (31.21°; solvents and H atoms were omitted for clarity).

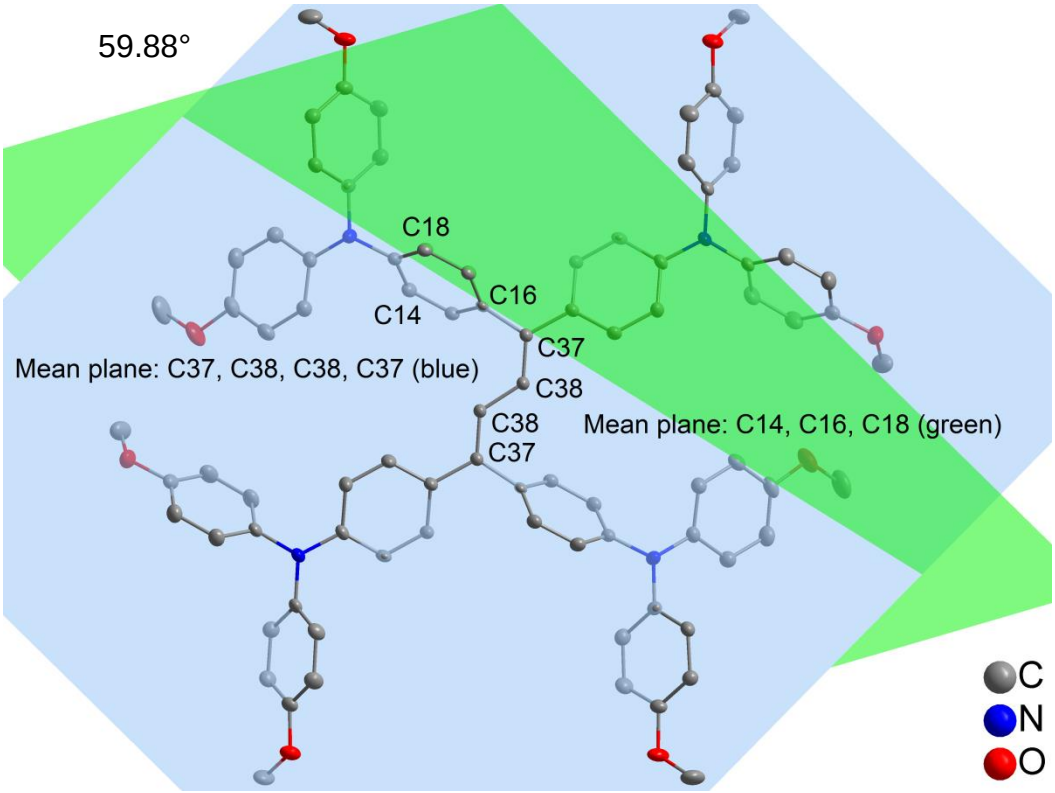

Figure S37. Dihedral angle between central butadiene and surrounding phenyl ring (59.88°; solvents and H atoms were omitted for clarity).

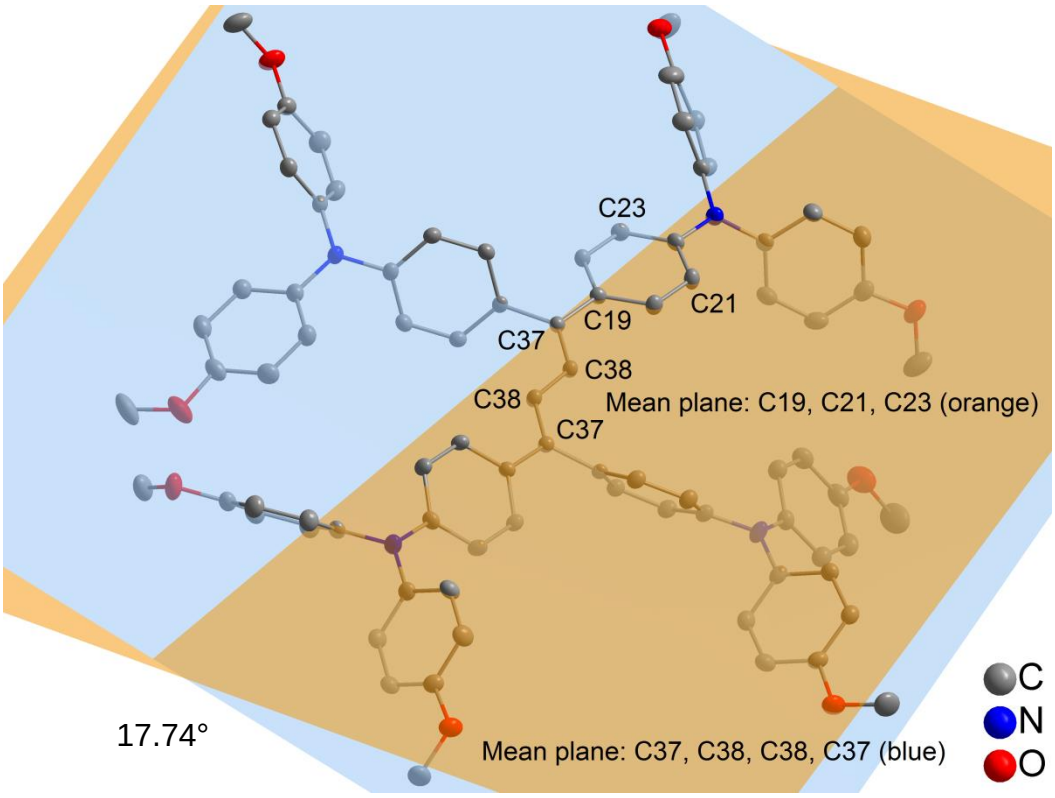

Figure S38. Dihedral angle between central butadiene and surrounding phenyl ring (17.74°; solvents and H atoms were omitted for clarity).

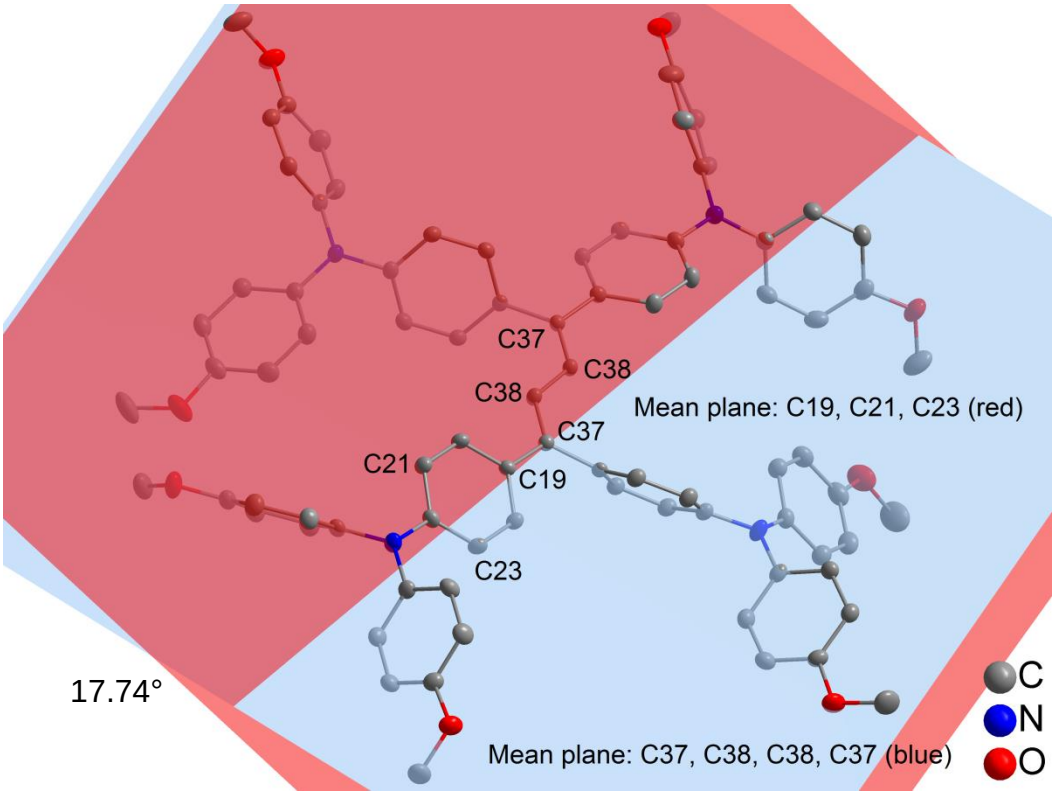

Figure S39. Dihedral angle between central butadiene and surrounding phenyl ring (17.74°; solvents and H atoms were omitted for clarity).

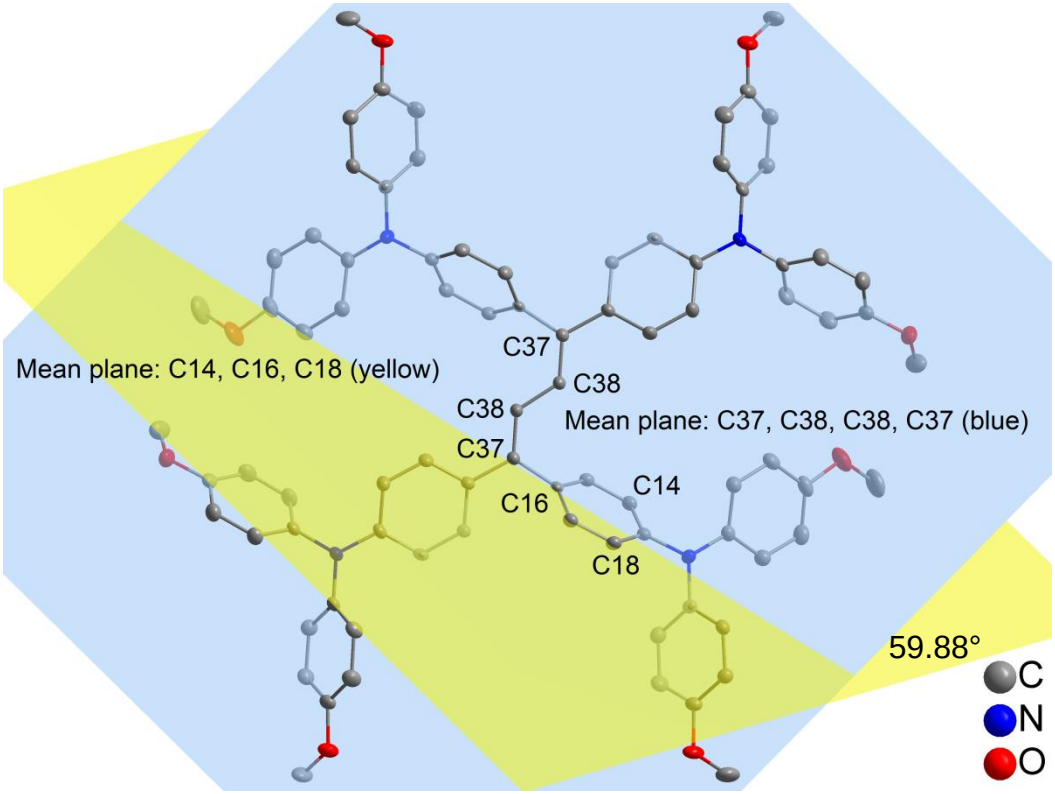

Figure S40. Dihedral angle between central butadiene and surrounding phenyl ring (59.88°; solvents and H atoms were omitted for clarity).

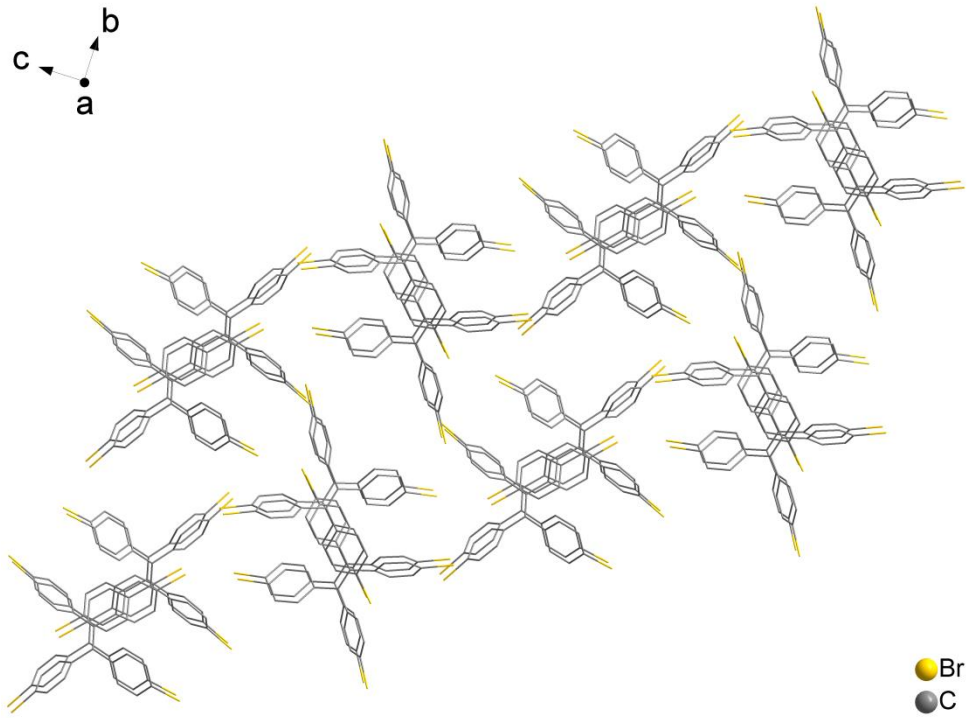

Figure S41. Stacking molecules of 1,1,2,2-tetrakis(4-bromophenyl)ethene (parallel and perpendicular to the *a* axis, respectively; solvents and H atoms were omitted for clarity).

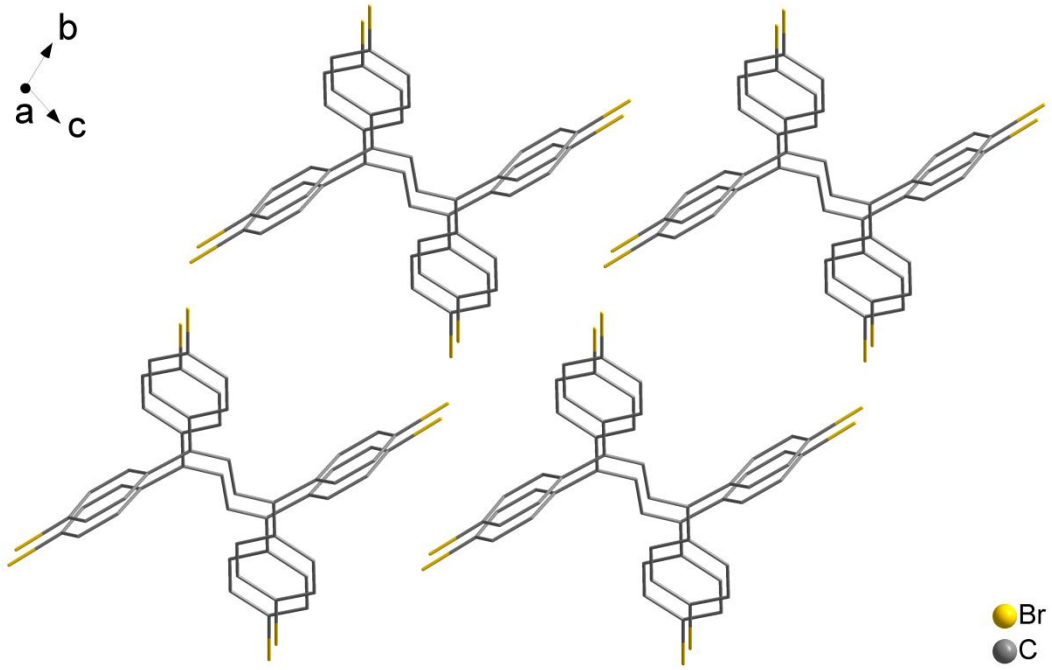

Figure S42. Stacking molecules of **4** (parallel and perpendicular to the *a* axis, respectively; solvents and H atoms were omitted for clarity).

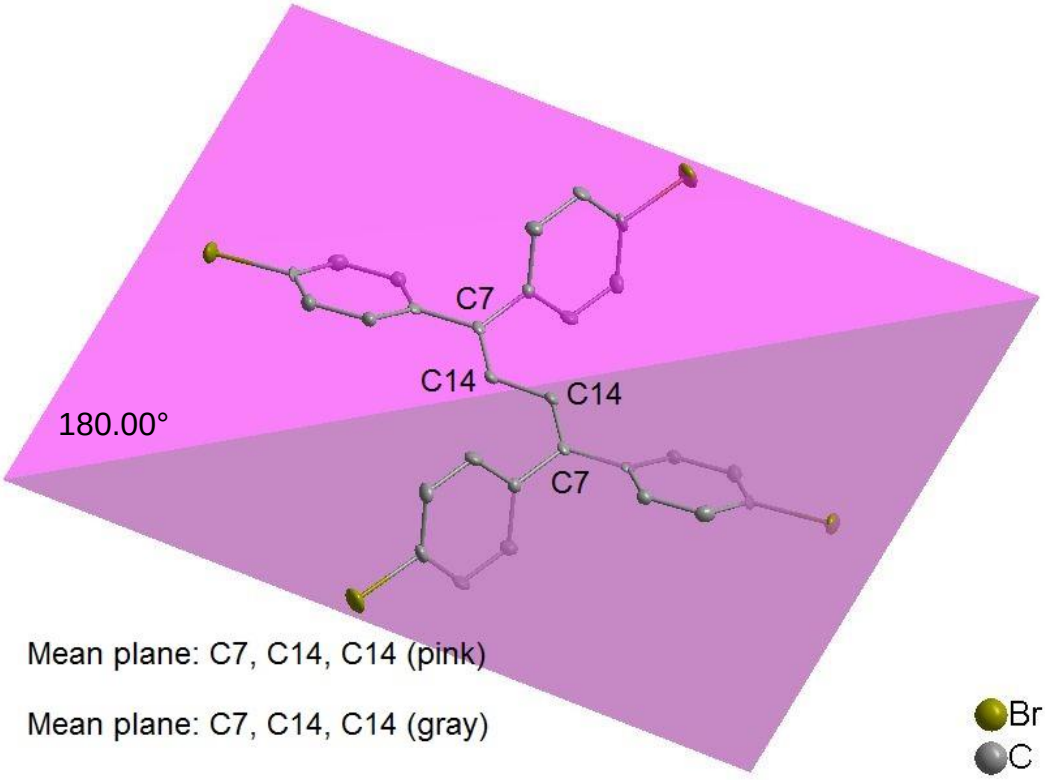

Figure S43. Torsion angle of the four C atoms in butadiene (180.00 °; solvents and H atoms were omitted for clarity).

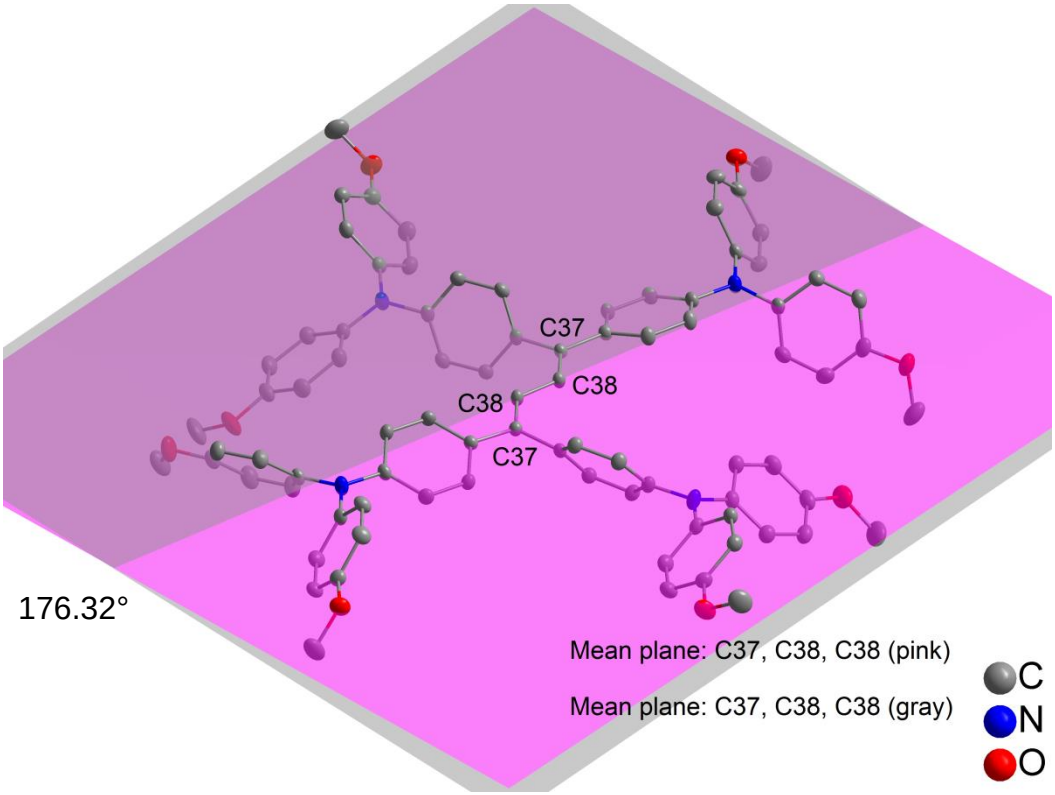

Figure S44. Torsion angle of the four C atoms in butadiene (176.32 °; solvents and H atoms were omitted for clarity).

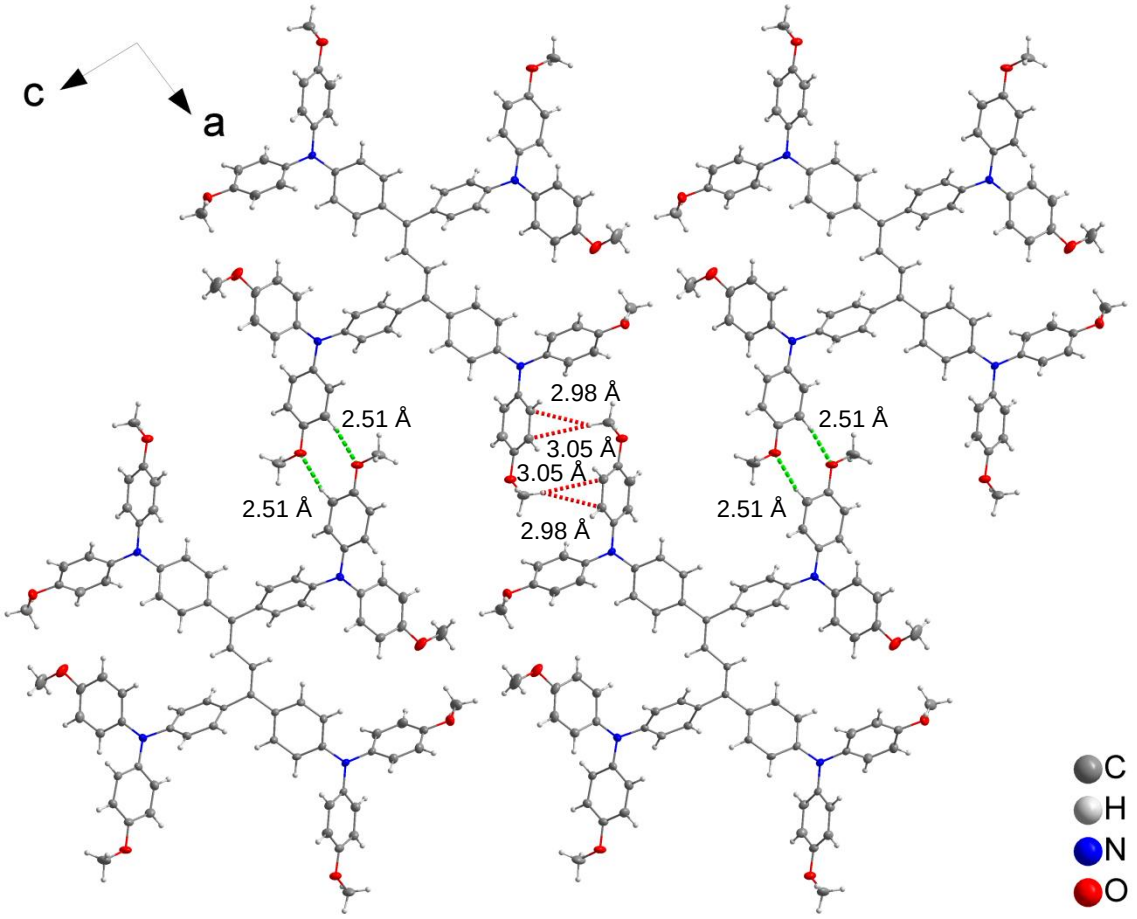

Figure S45. C–H···O Hydrogen bonds (dashed green lines) and CH/π interactions (dashed red lines) whitin a layer of **CJ-03** molecules (solvents were omitted for clarity).

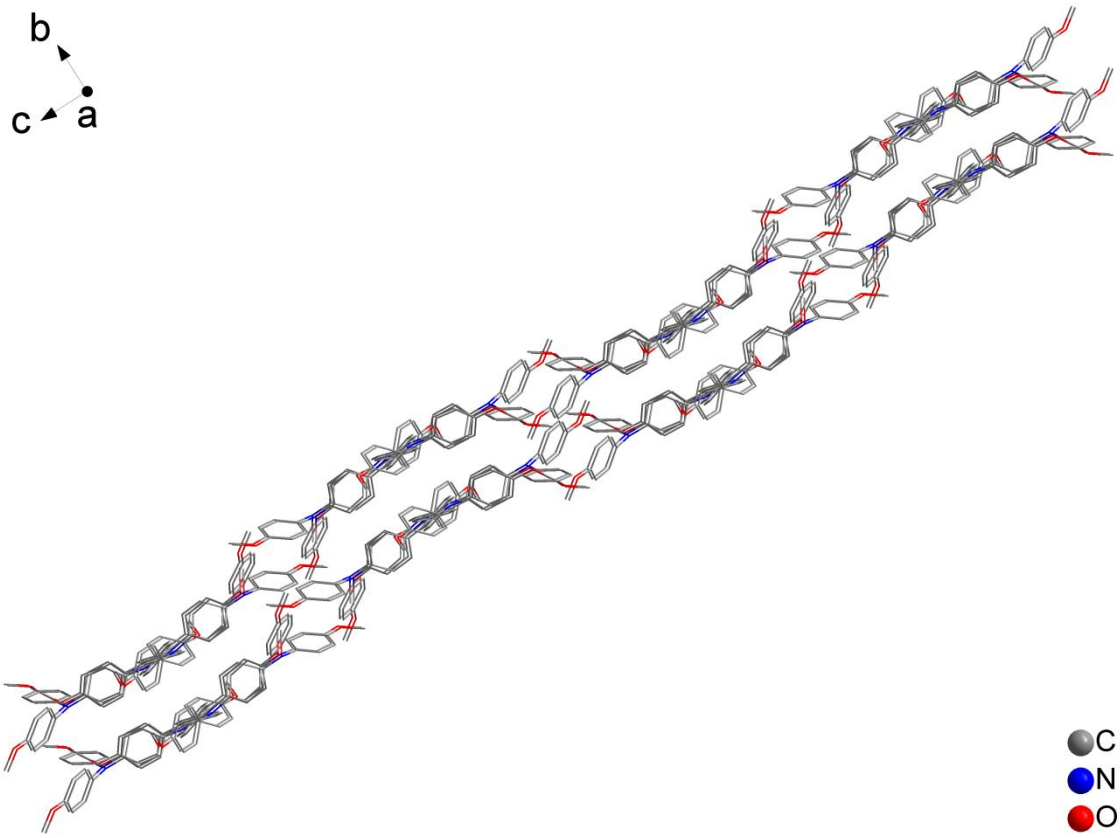

Figure S46. Stacking molecules of **CJ-03** (parallel and perpendicular to the *a* axis, respectively; solvents and H atoms were omitted for clarity).

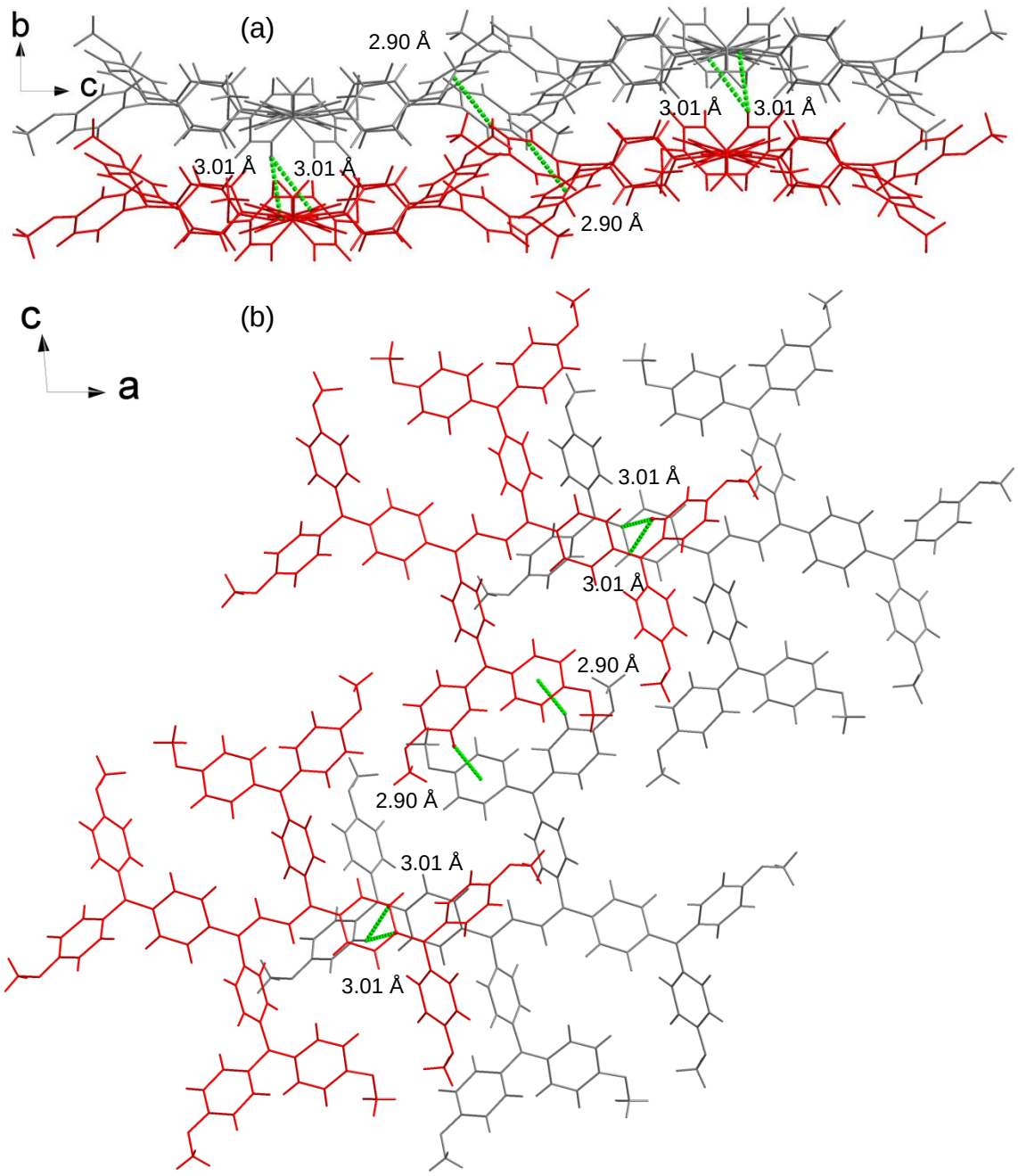

Figure S47. CH/π interactions (dashed green lines) between two layers of **CJ-03** molecules: (a) view down the *a* axis and (b) view down the *b* axis (solvents were omitted for clarity).

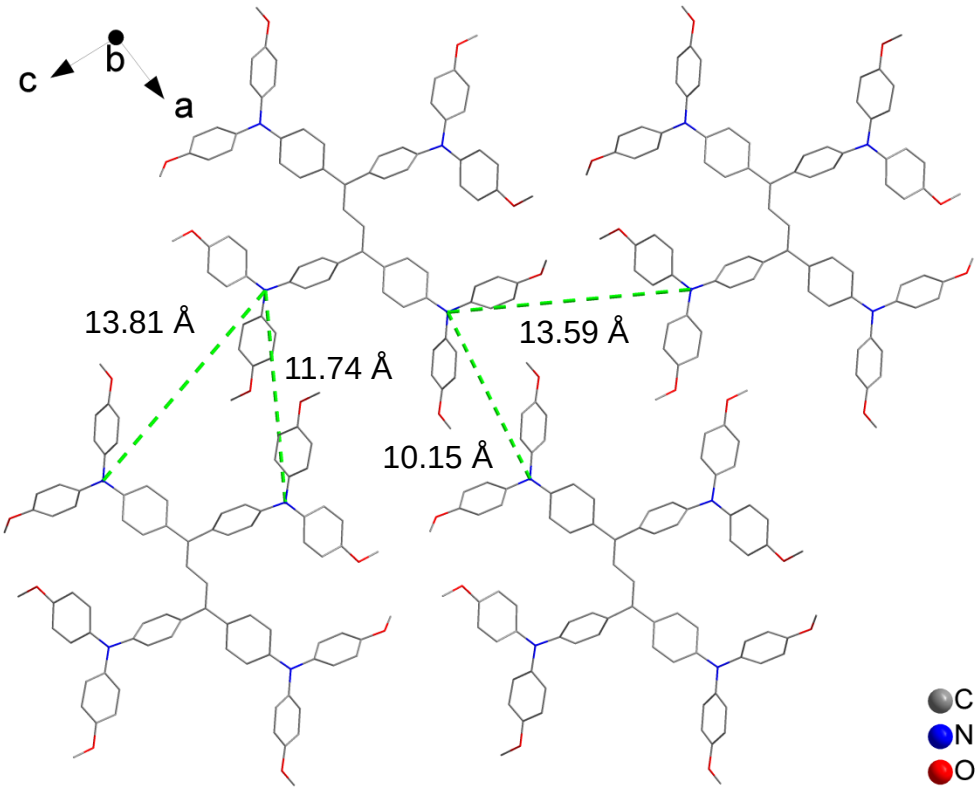

Figure S48. N–N distances whitin a layer of **CJ-03** molecules (dashed green lines; solvents and H atoms were omitted for clarity).

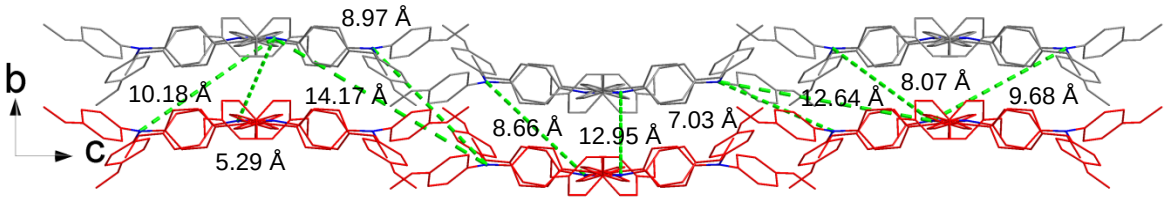

Figure S49. N–N distances between two layers of **CJ-03** molecules (dashed green lines; solvents and H atoms were omitted for clarity).

Table S6. Crystallographic data of **4** and **CJ-03**

Substance	**4**, tetrahydrofuran	**CJ-03**, CH_2Cl_2
Formula	$C_{28}H_{18}Br_4$, C_4H_8O	$C_{84}H_{74}N_4O_8$, 4 (CH_2Cl_2)
M_r	746.17	1607.18
Crystal color, habit	Colorless, block	Orange, block
Crystal system, space group	Triclinic, $P\bar{1}$	Monoclinic, $C2/c$
Radiation type, wavelength (Å)	Mo K_α, 0.71073	Cu K_α, 1.54184
Temperature (K)	150.00(10)	150.00(10)
Crystal size (mm)	0.6 × 0.3 × 0.2	0.35 × 0.12 × 0.05
a (Å)	6.4195(3)	24.3715(3)
b (Å)	10.8173(6)	8.78720(10)
c (Å)	11.1868(6)	37.3337(4)
α (°)	104.935(5)	90
β (°)	96.182(4)	95.6710(10)
γ (°)	106.722(5)	90
V (Å^3)	704.83(6)	7956.15(16)
ρ (calc., g cm^{-3})	1.758	1.342
Z	1	8
μ (mm^{-1})	5.734	3.067
N °of rflcn/unique	5607/3037	30175/7951
θ range (°)	3.33–27.00	3.645–74.182
Compl. to θ_{max} (%)	98.6	98.3
R_1/wR_2 [$I > 2\sigma(I)$]	0.0433/0.0961	0.0568/0.1553
R_1/wR_2 (all data)	0.0527/0.1021	0.0600/0.1589
Goof	1.054	1.042
R_{int}	0.0371	0.0344
Largest diff. peak and hole (eÅ^{-3})	0.946 and –1.148	0.906 and –0.983

9. Integrated area of steady-state PL and fitting parameters of time-resolved PL

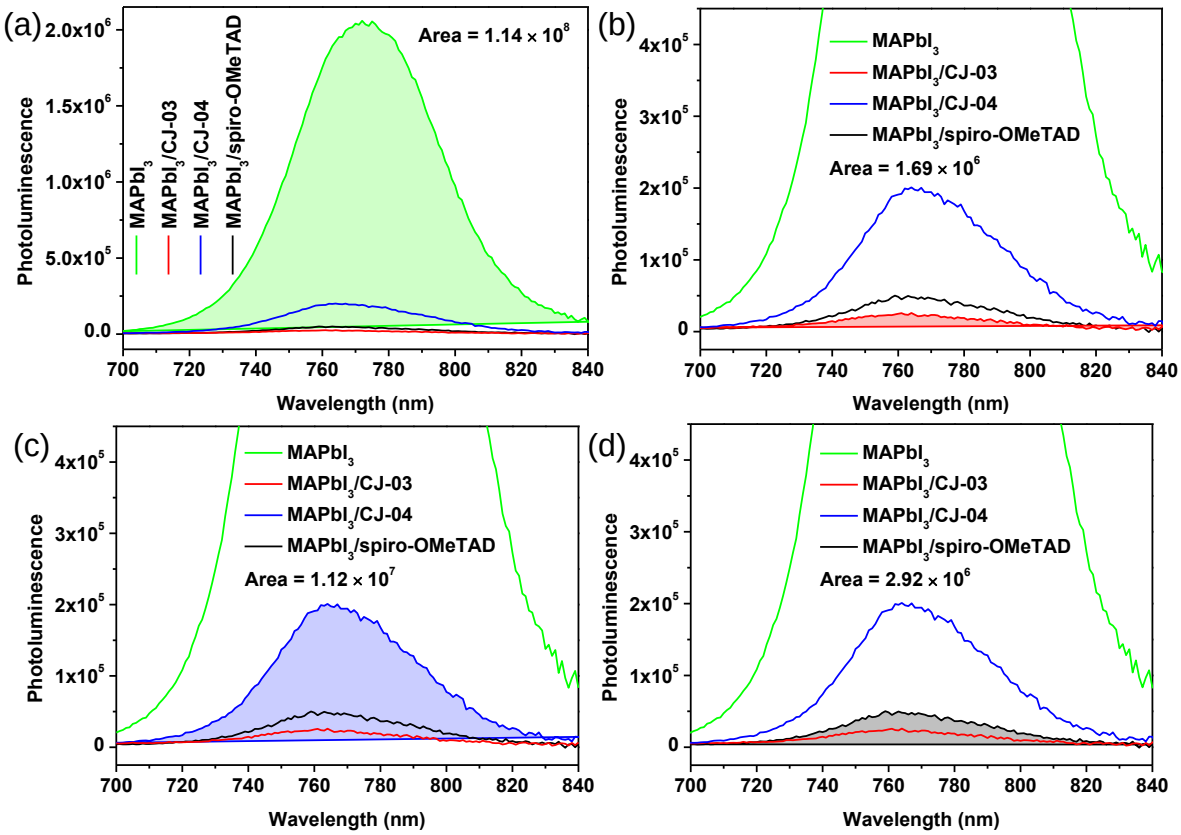

Figure S50. Integrated area of steady-state PL spectra: (a) $MAPbI_3$, (b) $MAPbI_3$/**CJ-03**, (c) $MAPbI_3$/**CJ-04**, and (d) $MAPbI_3$/spiro-OMeTAD.

Table S7. Summary of integrated area computed from steady-state PL spectra

Sample	Integrated area	Percentage (%)
$MAPbI_3$	1.14×10^8	100.00
$MAPbI_3$/**CJ-03**	1.69×10^6	1.48
$MAPbI_3$/**CJ-04**	1.12×10^7	9.82
$MAPbI_3$/spiro-OMeTAD	2.92×10^6	2.56

Table S8. Double-exponential fitting parameters of time-resolved PL spectra

Sample	τ_1 (ns)	frac. 1	τ_2 (ns)	frac. 2	ave. (ns)
$MAPbI_3$	7.38	9.09%	134.46	90.91%	122.91
$MAPbI_3$/**CJ-03**	2.56	38.56%	14.87	61.44%	10.12
$MAPbI_3$/**CJ-04**	3.87	21.65%	62.38	78.35%	49.71
$MAPbI_3$/spiro-OMeTAD	3.33	44.35%	26.90	55.65%	16.45

10. Hydrophobic properties

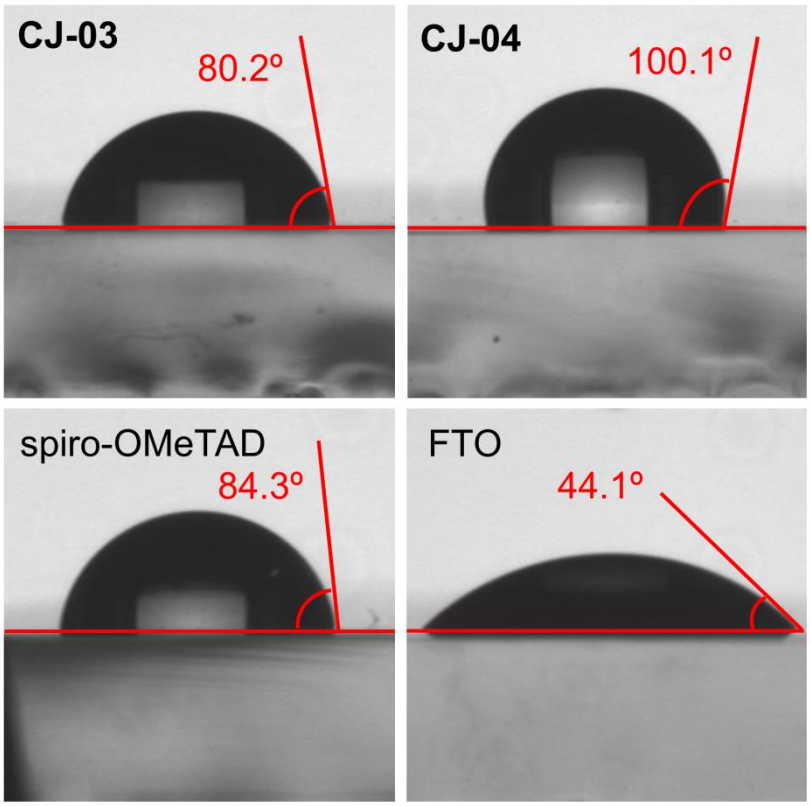

Figure S51. Water contact angles of HTM films spin-coated on fluorine-doped tin oxide (FTO) glass and water contact angle of naked FTO.

11. Film topography of HTMs with dopants

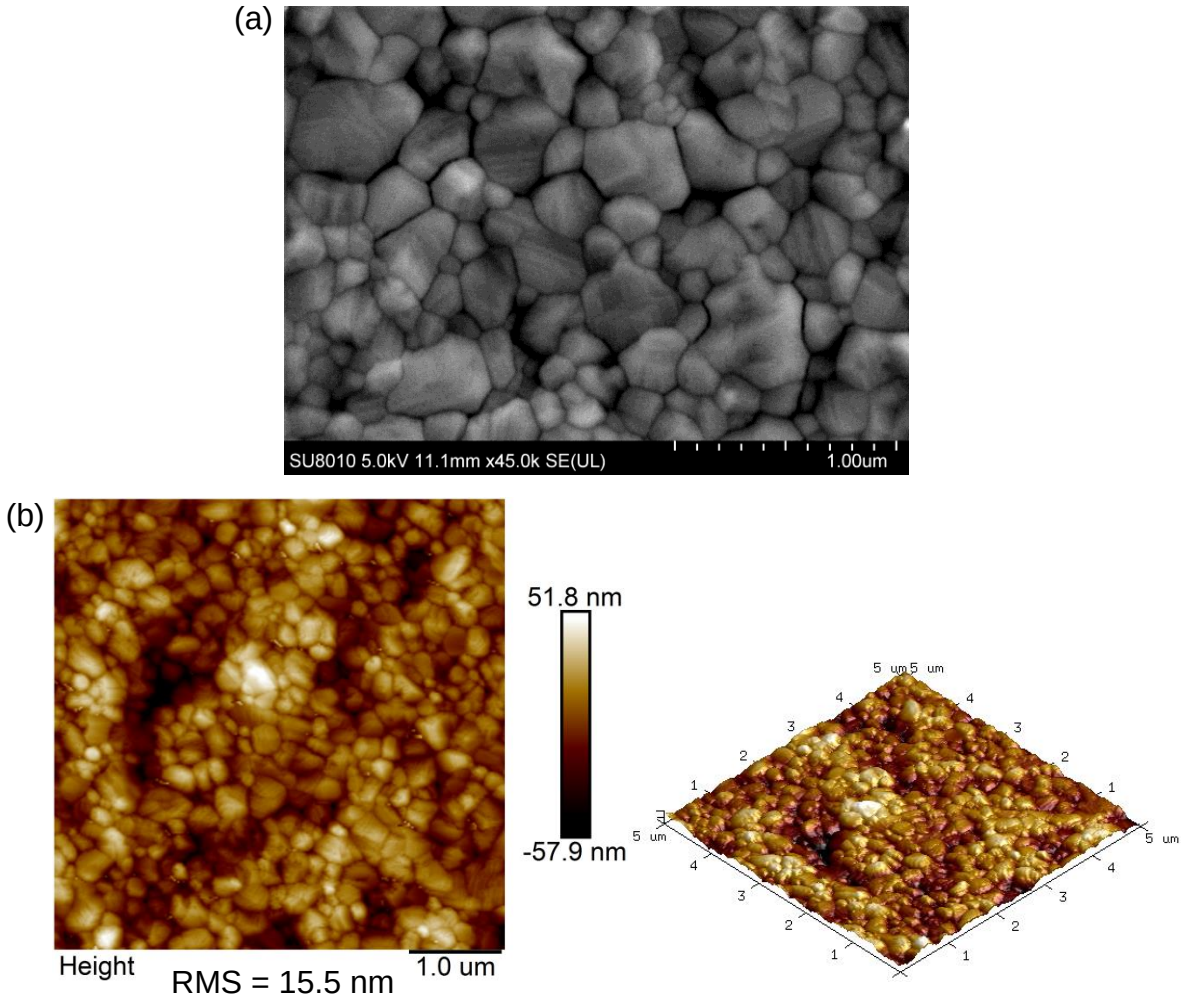

Figure S52. (a) SEM top-view picture of $MAPbI_3$. (b) AFM height and relevant 3D images of $MAPbI_3$.

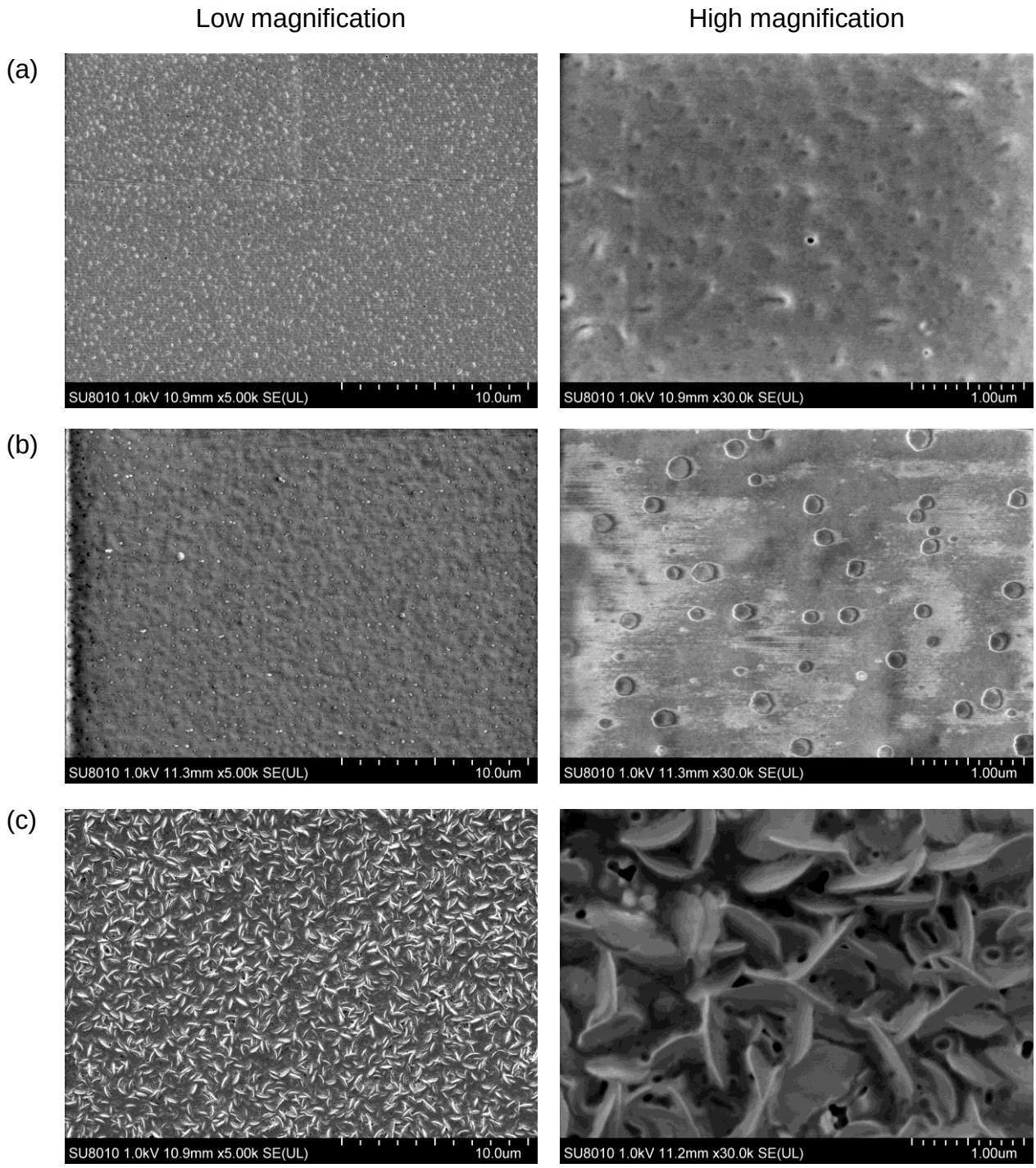

Figure S53. SEM top-view pictures of doped HTM films spin-coated on $MAPbI_3$: (a) **CJ-03**, (b) **CJ-04**, and (c) spiro-OMeTAD.

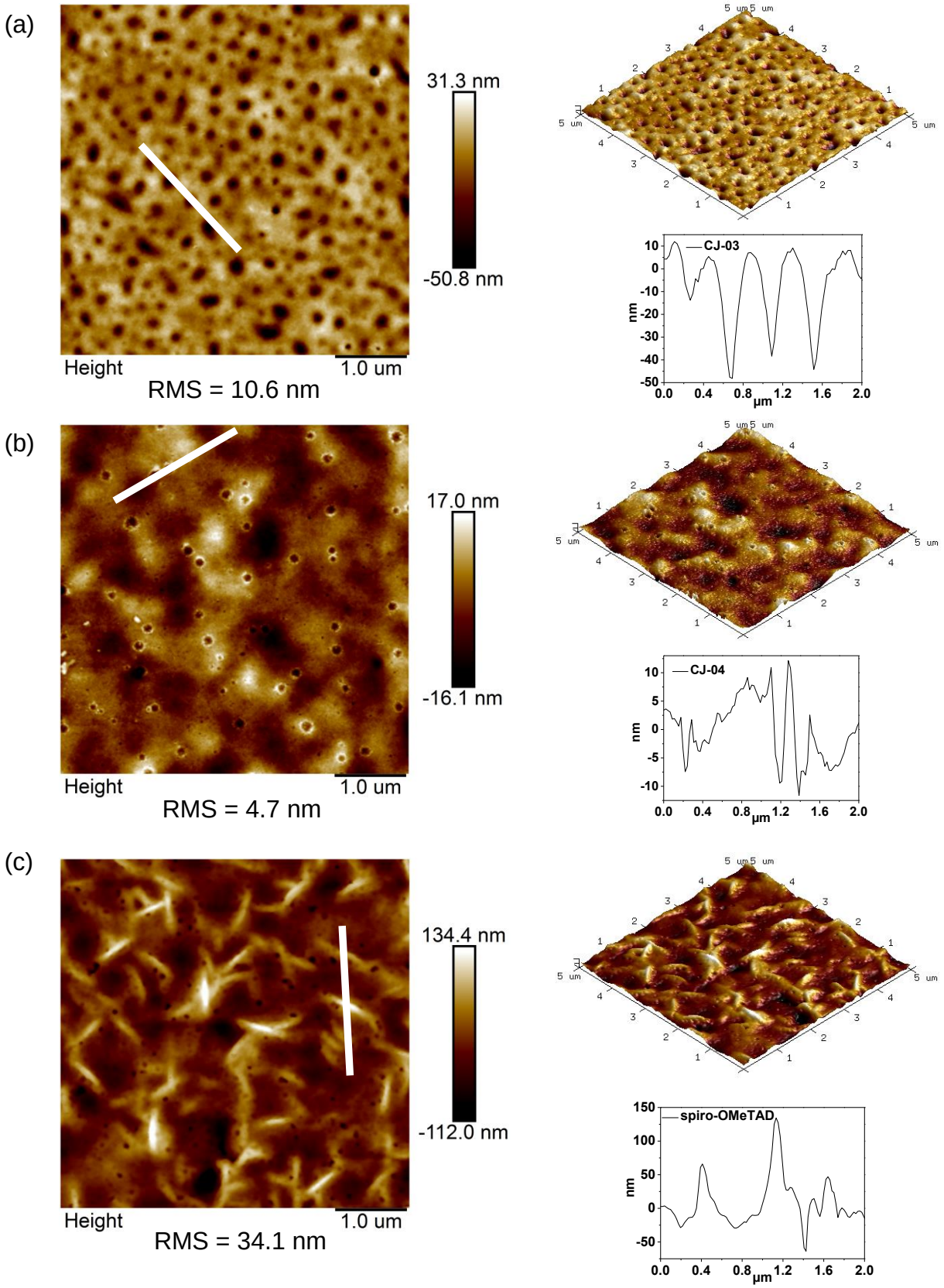

Figure S54. AFM height and relevant 3D images of doped HTM films spin-coated on $MAPbI_3$: (a) **CJ-03**, (b) **CJ-04**, and (c) spiro-OMeTAD.

12. Manufacture, tests, and performance data of perovskite solar cells (PSCs)

The fabrication and tests of PSCs follow our early work.[5] For the sake of succinctness, only the different contents are provided below. The HTM solutions were prepared according to Table S9. The spiro-OMeTAD solution was stirred overnight and filtered with a 0.22 μm PTFE filter before spin-coating. For **CJ-03** and **CJ-04**, there was no filtration before use. Their solutions were heated to ~100 ℃ until complete dissolution and then spin-coated while hot. (Note: In the intervals of spin-coating, the solutions should be kept on the hot plate at 100 ℃ to avoid the unpleasant precipitate.)

Table S9. Preparation of HTM solutions

HTM	Concentration ($mg\ mL^{-1}$)	Li-TFSI (mg)	FK209 (15 mol %) (mg)	*t*-BP (μL)	Chlorobenzene (mL)
CJ-03	60.0	9.1	10.7	28.8	1
CJ-04	60.0	9.1	8.6	28.8	1
spiro-OMeTAD	72.3	9.1	13.3	28.8	1

Table S10. Performance data of PSCs based on different HTMs derived from *J–V* curves (reverse scan)

HTM	Cell No.	J_{SC} (mA cm^{-2})	V_{OC} (V)	FF (%)	PCE (%)	R_s (Ω cm^{-2})
CJ-03	1	23.21	1.103	72.6	18.59	3.2
	2	22.92	1.075	75.3	18.55	2.9
	3	23.23	1.113	75.5	19.51	3.1
	4	23.26	1.108	73.0	18.81	3.1
	5	22.40	1.120	74.4	18.66	4.1
	6	22.74	1.101	72.1	18.05	3.7
	7	23.29	1.113	74.7	19.36	3.6
	8	23.06	1.113	74.7	19.17	3.5
	9	22.90	1.115	75.8	19.36	3.2
	10	23.08	1.115	77.3	19.90	2.9
	11	23.10	1.079	74.0	18.43	4.1
	12	22.88	1.055	75.3	18.17	3.6
	13	22.90	1.068	75.6	18.50	3.7
	14	22.92	1.073	75.4	18.55	3.7
	15	23.05	1.081	76.5	19.07	3.7
	16	22.93	1.075	76.4	18.83	3.6
	17	23.43	1.075	76.3	19.21	3.6
	18	22.84	1.074	76.4	18.74	3.7
	19	23.25	1.071	76.3	18.99	3.7
	20	22.17	1.075	76.8	18.30	3.9
	21	22.06	1.058	73.6	17.18	3.9
	22	23.40	1.066	75.1	18.75	4.0
	23	23.26	1.064	74.4	18.41	3.8
	24	22.72	1.054	74.0	17.72	3.8
	25	23.52	1.107	70.2	18.28	6.4

26	22.99	1.115	73.1	18.75	5.3
27	22.89	1.111	78.9	20.06	2.9
Average	22.98 ±0.34	1.088 ±0.022	75.0 ±1.8	18.74 ±0.61	3.7 ±0.7

HTM	Cell No.	J_{SC} (mA cm^{-2})	V_{OC} (V)	FF (%)	PCE (%)	R_s (Ω cm^{-2})
CJ-04	1	17.06	1.089	67.6	12.56	5.7
	2	18.70	1.070	66.6	13.33	3.0
	3	18.36	1.035	68.6	13.04	6.2
	4	18.39	1.042	69.3	13.27	6.8
	5	18.51	1.032	67.7	12.92	7.3
	6	17.65	1.040	69.6	12.77	6.7
	7	17.60	1.037	68.5	12.51	7.1
	8	16.13	1.035	68.6	11.45	7.8
	9	16.31	1.064	70.6	12.25	5.6
	10	19.09	1.031	68.1	13.40	7.4
	11	18.29	1.056	70.3	13.58	5.9
	12	17.74	1.031	67.3	12.32	6.3
	13	17.50	1.041	68.7	12.51	7.1
	14	16.95	1.070	70.1	12.71	6.8
	15	17.23	1.066	72.5	13.31	5.6
	16	16.62	1.031	71.9	12.32	7.2
	17	19.22	0.981	69.7	13.14	8.5
	18	17.62	1.079	68.1	12.94	7.3
	19	17.25	1.088	67.6	12.69	8.8
	20	16.66	1.044	69.6	12.11	6.9
	21	16.79	0.995	69.2	11.56	8.4
	22	18.09	1.036	70.1	13.14	5.9
	23	17.24	1.027	68.2	12.07	8.0

24	16.88	1.065	69.9	12.57	9.2
25	16.47	1.053	72.0	12.49	6.2
26	16.77	1.052	73.3	12.93	4.9
27	18.85	1.052	69.3	13.75	7.7
Average	17.55 ±0.87	1.046 ±0.024	69.4 ±1.6	12.73 ±0.56	6.8 ±1.3

HTM	Cell No.	J_{SC} (mA cm^{-2})	V_{OC} (V)	FF (%)	PCE (%)	R_s (Ω cm^{-2})
spiro-OMeTAD	1	23.15	1.084	71.6	17.96	5.8
	2	22.93	1.065	73.1	17.86	4.2
	3	22.74	1.080	72.5	17.81	5.0
	4	23.08	1.056	73.6	17.94	3.6
	5	23.31	1.053	73.4	18.01	3.7
	6	23.08	1.049	73.4	17.76	3.5
	7	22.92	1.050	73.7	17.75	3.4
	8	22.94	1.052	73.3	17.70	3.4
	9	23.08	1.080	75.3	18.76	4.4
	10	22.72	1.055	74.7	17.90	4.1
	11	22.67	1.054	74.4	17.77	3.5
	12	22.92	1.080	73.0	18.07	4.9
	13	23.36	1.074	72.7	18.24	4.7
	14	22.60	1.092	76.6	18.90	3.9
	15	21.86	1.078	75.3	17.76	3.2
	16	22.18	1.077	74.1	17.71	3.2
	17	22.57	1.081	73.3	17.89	3.3
	18	22.28	1.073	74.2	17.73	2.9
	19	22.64	1.066	73.6	17.75	2.8
	20	21.88	1.085	75.5	17.92	2.7
	21	22.57	1.072	73.3	17.74	2.5

22	22.86	1.069	72.2	17.64	2.6
23	22.73	1.061	74.1	17.87	2.9
24	22.57	1.072	73.8	17.85	2.7
25	22.19	1.077	74.6	17.84	2.7
26	22.20	1.075	74.6	17.81	2.9
27	22.43	1.080	73.5	17.81	4.6
Average	22.68 ±0.39	1.070 ±0.012	73.8 ±1.1	17.92 ±0.29	3.6 ±0.8

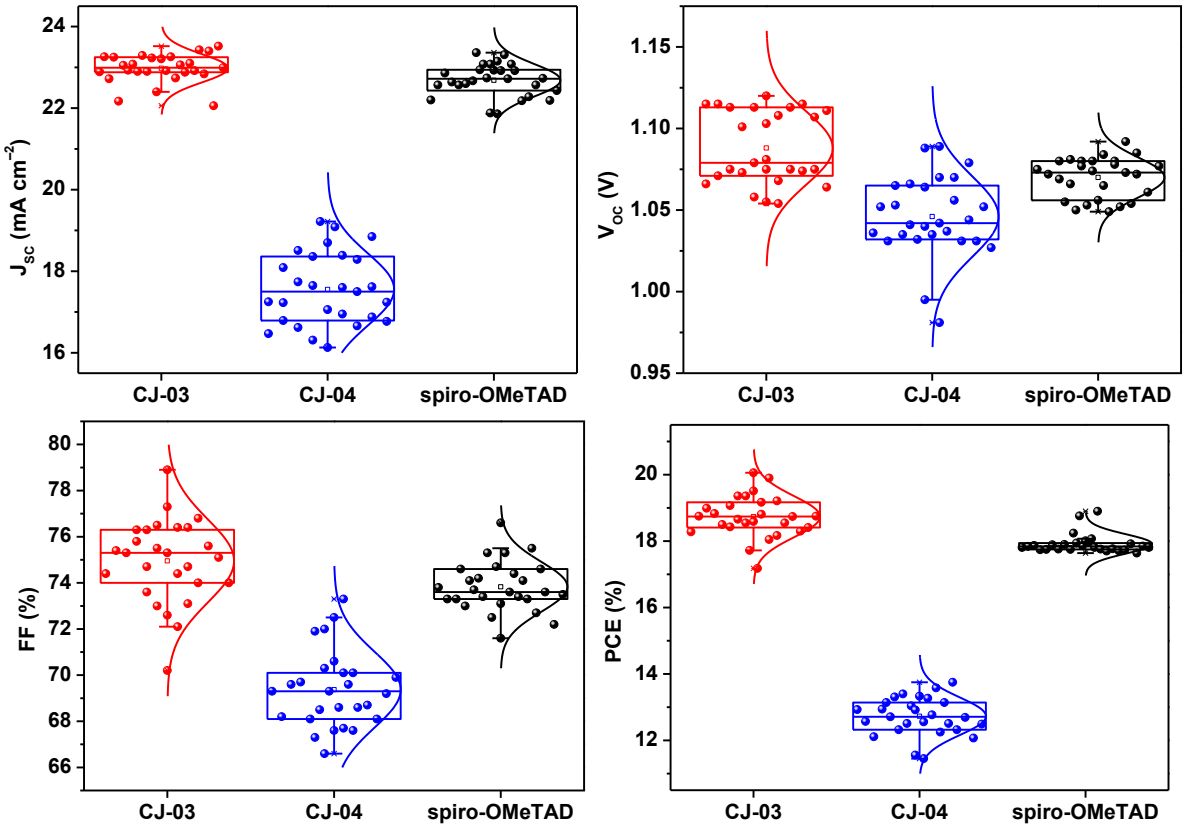

Figure S55. Performance statistics of PSCs (27 cells in several batches).

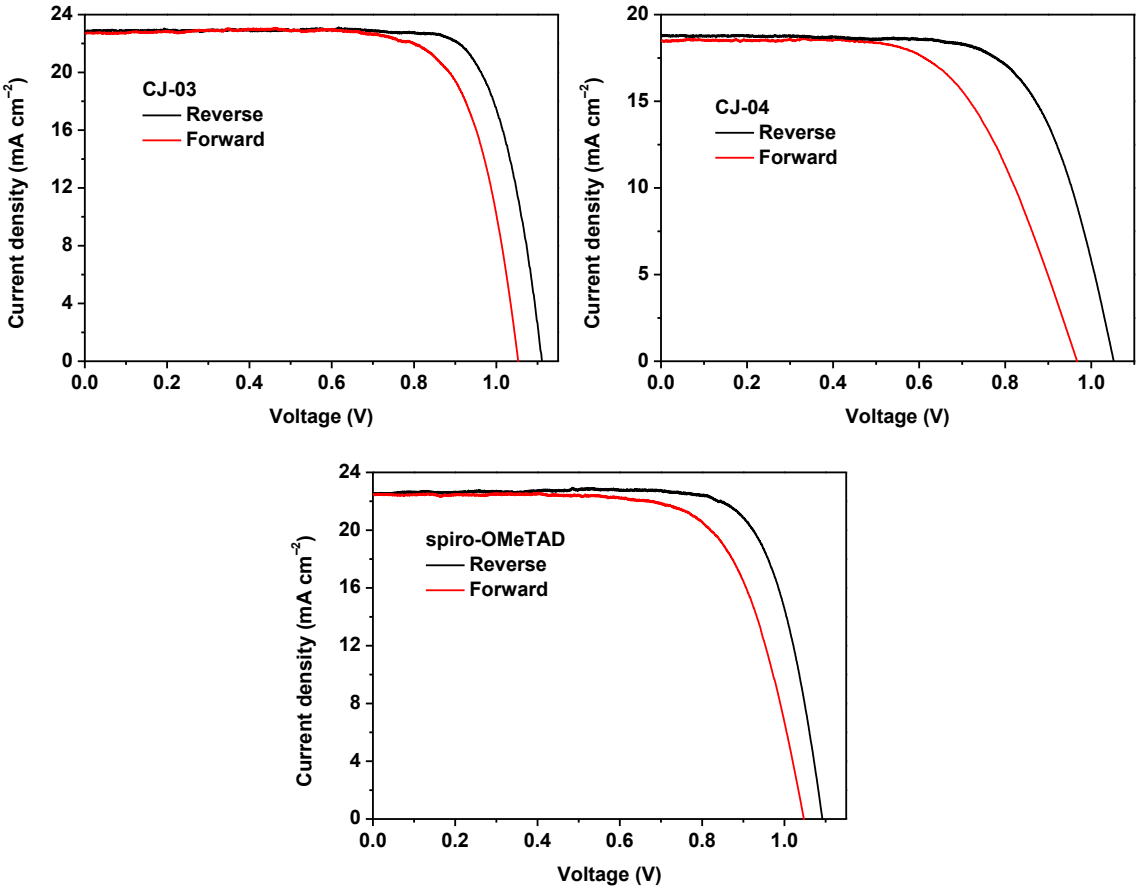

Figure S56. *J*–*V* curves of PSCs under reverse and forward scan at a voltage step of 1 mV and a scan rate of 200 mV/s.

Table S11. Performance data and hysteresis index of PSCs derived from *J*–*V* curves (reverse and forward scan)

HTM	Scan direction	J_{SC} (mA cm^{-2})	V_{OC} (V)	FF (%)	PCE (%)	Hysteresis index
CJ-03	Reverse	22.89	1.111	78.9	20.06	0.0486
	Forward	22.74	1.053	75.1	17.97	
CJ-04	Reverse	18.85	1.052	69.3	13.75	0.2113
	Forward	18.50	0.967	61.6	11.02	
spiro-OMeTAD	Reverse	22.60	1.092	76.6	18.90	0.0941
	Forward	22.43	1.047	70.2	16.49	

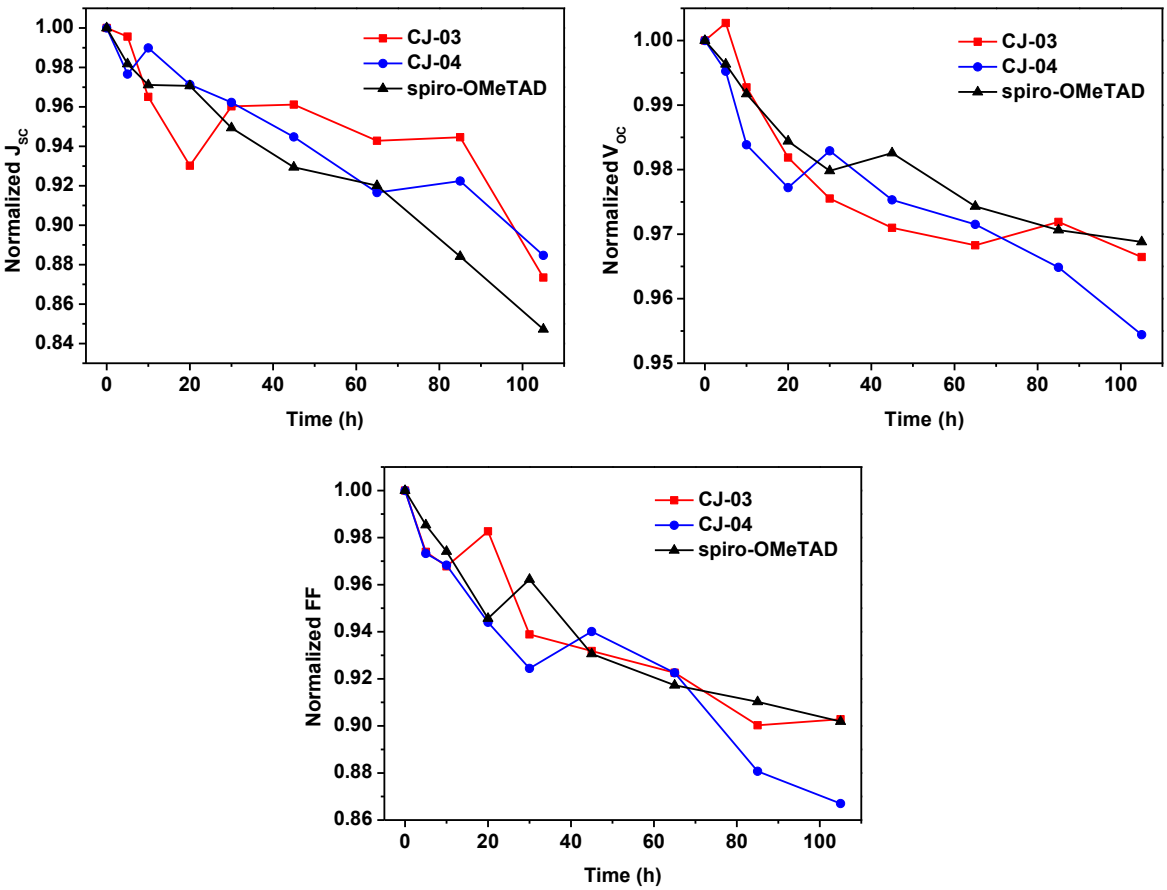

Figure S57. Time-course changes in the normalized J_{SC}, V_{OC}, and FF derived from *J*–*V* curves [without encapsulation in air, ~60% relative humidity (RH), 85 ℃].

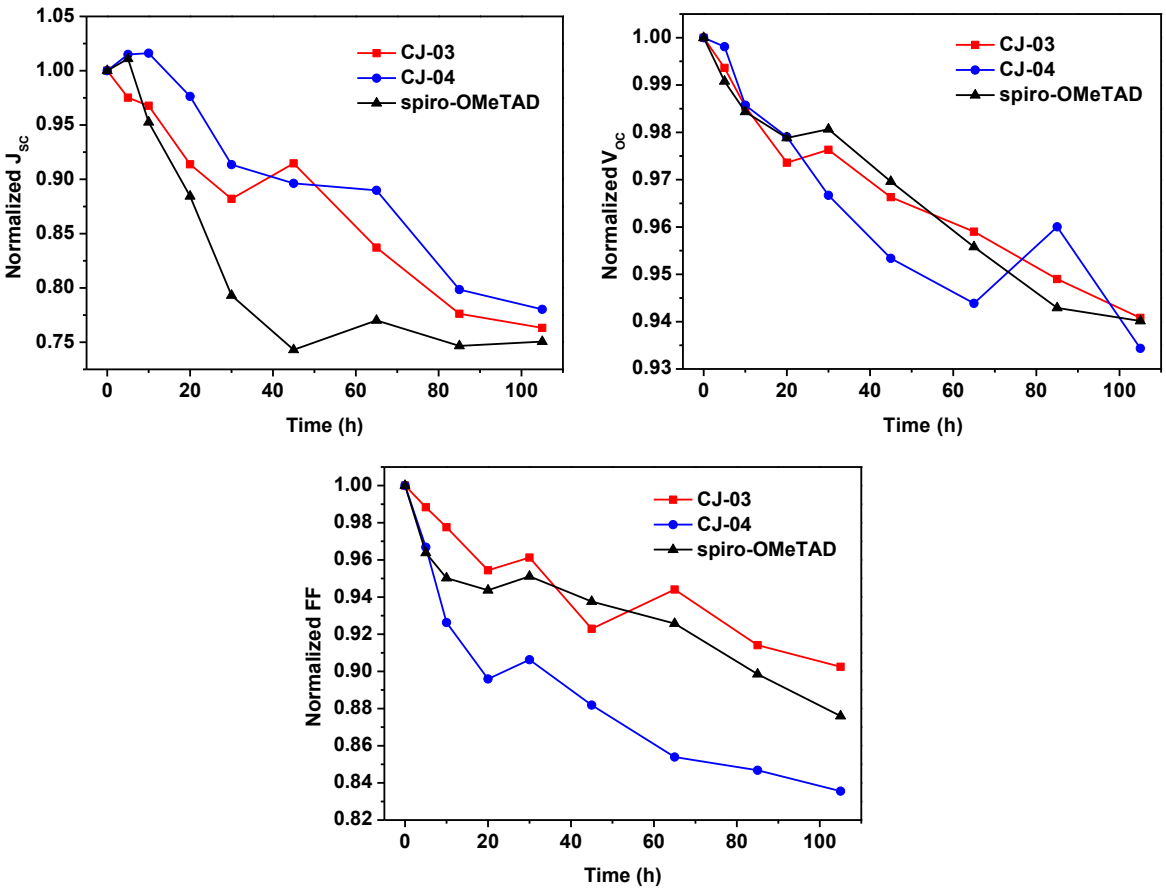

Figure S58. Time-course changes in the normalized J_{SC}, V_{OC}, and FF derived from *J*–*V* curves [without encapsulation in air, ~60% RH, AM 1.5 G irradiation (100 mW cm^{-2})].

13. Cost analysis for CJ-03

The following is an approximate cost evaluation based on a commonly cited method established by Osedach *et al.*[7]

(1) Extraction. 150 mL of DCM (3 × 50 mL) for extraction and 1 g of $MgSO_4$ for desiccation are assumed to be necessary to extract 1 g of crude product from a reaction mixture.

(2) Column chromatography. An ideal separation ration ($R_f \approx 0.2$) and sample loading are assumed. 60 g of silica gel and 1 L of eluent are assumed to be required to isolate 1 g product from the crude mixture.

(3) Recrystallization. We assume that 1 g of product needs 100 mL of solvent and the procedure is conducted only once.

The prices of each reagent (1 L or 1 kg) are gathered from http://www.tansoole.com/ (Titan, China, accessed: March, 2020). The amounts and expenses of reagents included in each synthetic step are tabulated in Table S12. The preparation expense of **CJ-03** is 153.91 CNY/g (22.95 USD/g). As this value does not take into account some inevitable aspects (for instance, expenditure of energy, disposal of waste, and manpower), it should be multiplied by 1.5 to obtain a more practical cost estimation (22.95 × 1.5 = 34.43 USD/g).[8] By comparison, the price of spiro-OMeTAD (99.5% purity) gleaned from http://www.p-oled.cn/ (Xi′an Polymer Light Technology Corp, China, accessed: March, 2020) is much higher (1000.00 CNY/g or 149.09 USD/g). CNY is short for Chinese Yuan. USD is the abbreviation of US Dollar.

Table S12. Cost estimation of **CJ-03** (1 g)

Chemical name	Weight (g)	Volume (mL)	Price (CNY for 1 Kg or 1 L)	Cost (CNY)	Sum (CNY)
4,4′-dibromobenzophenone	0.578	-	15925.00	9.20	
PPh_3CH_3Br	1.215	-	608.00	0.74	
t-BuOK	0.384	-	512.00	0.20	
Dry THF	-	6.804	200.00	1.36	19.92
silica gel	25.7	-	56.00	1.44	
petroleum ether	-	450	15.20	6.84	
ethyl acetate	-	9	16.00	0.14	
paraformaldehyde	0.057	-	64.00	0.01	
HBr (33 wt. % in acetic acid)	-	0.373	400.00	0.15	
CH_3COOH	-	4.980	20.00	0.10	
CH_2Cl_2 (extraction)	-	75	15.20	1.14	10.89
anhydrous $MgSO_4$	0.503	-	85.00	0.04	
silica gel	30.2	-	56.00	1.69	
petroleum ether	-	500	15.20	7.60	
ethyl acetate	-	10	16.00	0.16	

triethyl phosphite	-	0.405	176.00	0.07	8.98
silica gel	28.2	-	56.00	1.58	
petroleum ether	-	235	15.20	3.57	
ethyl acetate	-	235	16.00	3.76	
4,4′-dibromobenzophenone	0.360	-	15925.00	5.73	18.09
NaH (60% dispersion in mineral oil)	0.117	-	339.20	0.04	
dry THF	-	2.467	200.00	0.49	
silica gel	38.0	-	56.00	2.13	
petroleum ether	-	580	15.20	8.82	
CH_2Cl_2	-	58	15.20	0.88	
4,4′-dimethoxydiphenylamine	1.034	-	38176.00	39.47	96.03
$Pd(OAc)_2$	0.032	-	201600.00	6.45	
$(t\text{-Bu})_3P$ in toluene (300 mg/mL)	-	0.437	54264.00	23.71	
t-BuONa	1.811	-	339.20	0.61	
toluene	-	23.453	18.80	0.44	
silica gel	60.0	-	56.00	3.36	
petroleum ether	-	800	15.20	12.16	
THF	-	200	42	8.40	
CH_3OH (recrystallization)	-	20	10.40	0.21	
CH_2Cl_2 (recrystallization)	-	80	15.20	1.22	
-	-	-	-	-	153.91

References

(1) Fulmer, G. R.; Miller, A. J. M.; Sherden, N. H.; Gottlieb, H. E.; Nudelman, A.; Stoltz, B. M.; Bercaw, J. E.; Goldberg, K. I. *Organometallics* **2010**, *29*, 2176–2179.

(2) Frisch, M. J.; Trucks, G. W.; Schlegel, H. B.; Scuseria, G. E.; Robb, M. A.; Cheeseman, J. R.; Scalmani, G.; Barone, V.; Mennucci, B.; Petersson, G. A.; Nakatsuji, H.; Caricato, M.; Li, X.; Hratchian, H. P.; Izmaylov, A. F.; Bloino, J.; Zheng, G.; Sonnenberg, J. L.; Hada, M.; Ehara, M.; Toyota, K.; Fukuda, R.; Hasegawa, J.; Ishida, M.; Nakajima, T.;

Honda, Y.; Kitao, O.; Nakai, H.; Vreven, T.; Montgomery, J. A.; Jr., Peralta, J. E.; Ogliaro, F.; Bearpark, M.; Heyd, J. J.; Brothers, E.; Kudin, K. N.; Staroverov, V. N.; Kobayashi, R.; Normand, J.; Raghavachari, K.; Rendell, A.; Burant, J. C.; Iyengar, S. S.; Tomasi, J.; Cossi, M.; Rega, N.; Millam, J. M.; Klene, M.; Knox, J. E.; Cross, J. B.; Bakken, V.; Adamo, C.; Jaramillo, J.; Gomperts, R.; Stratmann, R. E.; Yazyev, O.; Austin, A. J.; Cammi, R.; Pomelli, C.; Ochterski, J. W.; Martin, R. L.; Morokuma, K.; Zakrzewski, V. G.; Voth, G. A.; Salvador, P.; Dannenberg, J. J.; Dapprich, S.; Daniels, A. D.; Farkas, O.; Foresman, J. B.; Ortiz, J. V.; Cioslowski, J.; Fox, D. J. Gaussian 09W, Version 7.0, Gaussian, Inc., Wallingford CT (**2009**).

(3) Dennington II, R. D.; Keith, T. A.; Millam, J. M. GaussView, Version 5.0.8, Gaussian, Inc., Wallingford CT (**2008**).

(4) Namai, H.; Ikeda, H.; Kato, N.; Mizuno, K. Substituent Effects on the Energies of the Electronic Transitions of Geminally Diphenyl-Substituted Trimethylenemethane (TMM) Radical Cations. Experimental and Theoretical Evidence for a Twisted Molecular and Localized Electronic Structure. *J. Phys. Chem. A* **2007**, *111*, 4436–4442.

(5) Chen, J.; Xia, J.-X.; Yu, H.-J.; Zhong, J.-X.; Wu, X.-K.; Qin, Y.-S.; Jia, C.-Y.; She, Z.-G.; Kuang, D.-B.; Shao, G. Asymmetric 3D Hole-Transporting Materials Based on Triphenylethylene for Perovskite Solar Cells. *Chem. Mater.* **2019**, *31*, 5431–5441.

(6) Tanaka, K.; Fujimoto, D.; Altreuther, A.; Oeser, T.; Irngartinger, H.; Toda, F. Chiral Inclusion Crystallization of Achiral Tetrakis(*p*-halophenyl)ethylenes with Achiral Guest Compounds. *J. Chem. Soc., Perkin Trans. 2* **2000**, 2115–2120.

(7) Osedach, T. P.; Andrew, T. L.; Bulović, V. Effect of Synthetic Accessibility on the Commercial Viability of Organic Photovoltaics. *Energy Environ. Sci.* **2013**, *6*, 711–718.

(8) Saliba, M.; Orlandi, S.; Matsui, T.; Aghazada, S.; Cavazzini, M.; Correa-Baena, J.-P.; Gao, P.; Scopelliti, R.; Mosconi, E.; Dahmen, K.-H.; De Angelis, F.; Abate, A.; Hagfeldt, A.; Pozzi, G.; Grätzel, M.; Nazeeruddin, M. K. A Molecularly Engineered Hole-Transporting Material for Efficient Perovskite Solar Cells. *Nat. Energy* **2016**, *1*, 15017.